Cdhr1a and pcdh15b link photoreceptor outer segments with inner segment calyceal processes revealing a potential mechanism for cone-rod dystrophy.

Meet K. Patel[1], Warlen Piedade[1] and Jakub K. Famulski[1*]

1) Department of Biology, University of Kentucky

* corresponding author

ABSTRACT

Cone rod dystrophy (CRD) is a macular degeneration disorder characterized by initial cone cell photoreceptor degeneration and subsequently of rod photoreceptors. Mutations in CDHR1, a photoreceptor specific cadherin have been found to be associated with the incidence of cone-rod dystrophy and recapitulated in mouse CDHR1 knockouts. However, the molecular function of CDHR1 remains unknown. CDHR1 has been shown to localize at the leading edge of murine rod nascent outer segment (OS) making junctions to an unknown partner in the inner segment. Using Structured Illumination Microscopy (SIM), we observed that the localization of zebrafish cdhr1a extends from basal nascent OS discs above the periciliary ridge of the inner segment to a considerable length along the OS, akin to calyceal process (CPs). When labeling the CPs using pcdh15b, a CP specific cadherin, we observed that cdhr1a at the leading edge of OS juxtaposes with pcdh15b in the CP. Similar localization patterns were detected in human, macaque, xenopus, ducks, and various rodent PRCs indicating conservation. Importantly, using immunoprecipitation and K652 cell aggregation assays we demonstrate that pcdh15b and cdhr1a can interact and potentially link the OS and CP. To analyze the consequences of OS-CP interactions in CRD, we established a zebrafish *cdhr1a* mutant line (*cdhr1a*^{fs*146}) and analyzed CRD progression at high temporal resolution. Homozygous *cdhr1a*^{fs*146} mutants begin to exhibit minor cone OS morphology defects starting at 15 dpf (days post fertilization) and severe OS disruption and cell loss by 3 months. Rod OS defects were delayed until 3-6 months. Furthermore, we show that loss of cdhr1a function leads to disorganization and shortening of CPs coinciding with cone outer OS defects which is significantly exacerbated when combined with the loss of pcdh15b. In conclusion, we propose that cdhr1a and pcdh15b function to link cone OSs with CPs to maintain proper OS homeostasis thus revealing a potential novel mechanism for CRD.

Keywords: cone-rod dystrophy, cdhr1, calyceal process, pcdh15

INTRODUCTION

Inherited retinal diseases (IRDs) are a group of disorders that can severely affect vision and even lead to blindness affecting over 450,000 individuals in the US alone [1]. Cone Rod dystrophy is a subset of IRD that leads to cone PRC degeneration followed by decline of rod PRCs [1,2]. The disorder generally stems from mutations in one of the over 30 gene candidates. Function of a putative CRD candidate, CDHR1 has been known to clinically correlate with recessive cone rod dystrophy [3-5]. CDHR1, a photoreceptor-specific cadherin, was first investigated by Rattner and colleagues in 2001 (previously PCDH21) where it was shown that a mouse KO resulted in early onset retinal degeneration, at one month and severe degeneration by six [6]. Subsequent studies have shown that initial retinal degeneration involves loss of cones and subsequently rods [7]. Molecularly, in the mouse model, it's been shown that CDHR1 localizes at the leading edge of OS discs and forms cadherin-based junctions to an unknown partner in the inner segment [6,8]. These connections have been hypothesized to regulate nascent rod OS disc release into the mature OS [9]. However, CDHR1 function in cones has not been postulated. In *Xenopus*, absence of Cdhr1 results in overgrown OS discs at the basal OS thereby disrupting the normal OS [10]. In humans, CDHR1 mutations, both truncations and missense mutations, have been shown to correlate with late onset CRD [5,11-13]. Clinically, these studies identify various pathogenic and variants of unknown significance, however the exact mechanism behind CDHR1 based CRD pathogenesis remains unknown.

CDHR1, like other cadherins encodes an intracellular domain, a transmembrane domain and six evolutionarily conserved extracellular cadherin domain repeats (EC repeats) [6,9]. The cytoplasmic domains of classical cadherins have been shown to bind beta catenin, which anchors the cadherin to various cytoskeletal elements such as actin [14]. Interestingly, the cytoplasmic domain of Cdhr1 diverges considerably from other cadherins and is predicted to not possess any beta catenin or cytoskeletal binding activity [9,15]. ECs of most cadherins possess negatively charged sequence motifs, which are involved in Ca^{2+} binding [16]. These ECs form either homophilic or heterophilic junctions in trans conformation and thereby mediate inter/intracellular connections [17]. Protocadherins generally consist of six to seven EC repeats and are predominantly observed with high diversity in various neuronal populations [18]. In neurons, protocadherins are responsible for synaptogenesis, neuronal specificity, and formation of mechanical junctions [19]. Based on mouse studies, CDHR1 forms connections with the IS to

what appears to be the periciliary ridge and an extension of the IS appearing to be the calyceal process [8].

Calyceal processes (CPs) were first described by Cohen *et al.* in 1961 (as calyx of a flower) surrounding the basal OS discs in rhesus macaque and pigeon photoreceptors [20]. Pioneering work in the 1970-80s showed these processes are actin-based microvilli projections of the IS found in both rods and cones of various vertebrates including zebrafish and humans [21,22]. In macaque PRCs, thicker, longer and more numerous CPs were observed surrounding cones versus rods [23]. Based on their proximity to the OS, CPs were hypothesized to structurally support the OS discs in both rods and cones [24]. However, functional evidence of their potential aid to the OS remains scarce. Previous studies also show how CPs are absent and a vestigial remanence of Periciliary ridge extension is observed in popular rodent models such as mice and rats, which may suggest to the lack of functional evidence of CPs [23,25]. Studies in macaque PRCs indicated localization of various Usher syndrome 1 (Ush1) proteins to the calyceal processes [23]. Clinically Usher syndrome 1 is categorized by loss of hearing and vision due to mutations in one of the six Ush1 genes [26]. Of these six Ush1 genes, Pcdh15 has been shown to make heterophilic cadherin-based junctions in stereocilia of hair cells with another Ush1 gene, Cadherin 23 (Cdh23) [27]. Thereby they form a mechanical bridge between adjacent stereocilia. Mechanical deflection of stereocilia due to sound waves changes the tension of Pcdh15-Cdh23 based interactions, which then triggers the mechano-electrical transduction channel for signal propagation [28,29]. Loss of functional Pcdh15 results in Usher syndrome type 1f, entailing the loss of hearing and vision [30]. In PRCs, Pcdh15 has been unequivocally shown to be localized in the CPs [23,31,32]. Interestingly loss of pcdh15b function in zebrafish results in an abnormal OS phenotype and PRC degeneration [31]. However, the mechanism of pcdh15b based PRC pathogenesis remains unknown. Noting the expression of two retinal cadherins in juxtaposing structures, CDHR1 in the OS and PCDH15 in the CP, we sought out to investigate whether CDHR1 and PCDH15 interact to link the OS discs and the CP.

In our current study we demonstrate that in zebrafish PRCs cdhr1a and pcdh15b juxtapose along the OS and CP suggesting they form functional connections. Importantly, we show that this localization pattern is evolutionarily conserved up to and including humans. Furthermore, we confirm pcdh15b-cdhr1a interactions via immunoprecipitation and K562 cell aggregation. While modeling CRD using a cdhr1a loss of function mutant line we report progressive defects in CP

112 morphology correlating specifically with cone degeneration. Taken together, we propose that
113 loss of cdhr1a function disrupts OS-CP junctions and subsequently leads to CRD.
114
115 **RESULTS**
116 **Cdhr1a localization in the OS suggests an interaction with the calyceal process.**
117 As previously mentioned, CDHR1 has been shown to localize to the inner/outer segment
118 boundary in several species, and in mouse rod cells it was shown to extend from newly formed
119 discs and form linkages with the inner segment. The connecting partner had yet to be
120 determined. To expand our understanding of CDHR1 localization we performed IHC for cdhr1a
121 and imaged the sections using high resolution confocal microscopy. When focusing on cone
122 cells, we observed that cdhr1a was not restricted to the IS/OS boundary, instead cdhr1a
123 localization was found along the edges of OSs (Fig 1A). Conversely in rod cells we observed
124 that cdhr1a localization was restricted to a much smaller region of the OS and closely
125 associated with the IS more reminiscent of the mouse cryo-EM studies (Fig 1B). The cone
126 pattern of localization was reminiscent of recent work showcasing the actin based IS extensions
127 called calyceal processes (CP). While little is known about the exact molecular function of CPs,
128 recent studies have shown that the Usher syndrome-associated protein pcdh15b, also a
129 protocadherin, localizes to the CP in zebrafish, and in non-human primates. After examining
130 zebrafish retinal expression of 5 key Usher proteins (Pcdh15b, Cdh23, Myo7a, Ush1c, and
131 Ush1g) we only detected pcdh15b in the PRC layer (Fig S1). Thus, using IHC we compared
132 cdhr1a localization to that of pcdh15b and excitedly observed a close association between the
133 two signals in both rods and cones (Fig 1A", B"). Interestingly, the localization of cdhr1a and
134 pcdh15b did not appear to directly overlap, thus suggesting that the two proteins may juxtapose
135 one another. To examine their localization at higher resolution, we turned to the super resolution
136 technique structured illumination microscopy (SIM). Using SIM, we confidently confirmed that
137 cdhr1a and pcdh15b signals juxtapose along the OS and the CP respectively (Fig 1C). The
138 similar length and vertical distribution of each signal corresponded to the other suggested they
139 may be interacting. Based on this observation, and the fact that both proteins are from the
140 cadherin family, we hypothesized that cdhr1a connects the OS to the CP by cadherin-based
141 interactions with pcdh15b (Fig 1D). To determine if this hypothesis pertains only to teleost fish,
142 we also examined localization of CDHR1 and PCDH15 across various vertebrate species
143 including frog, duck, mouse, rat, gerbil, spiny mouse, macaque and human (Fig 1E-L). In all the
144 species examined we observed a close localization or juxtaposition of Cdhr1 and Pcdh15

145 signals indicating that their association is likely to be evolutionarily conserved. Furthermore, as
146 was observed in zebrafish, in all the species examined the vertical distribution and pattern of
147 Cdhr1 signal always mirrored that of Pcdh15. Taken together, we postulated that the function of
148 Cdhr1 may be to link the OS discs to the CP and that loss of this interaction may represent a
149 mechanism of cone-rod dystrophy.
150
151 **Cdhr1a and pcdh15b interact and form functional connections.**
152 To test our hypothesis that cdhr1a and pcdh15b physically interact to connect the OS and CP
153 we first assessed their interaction using immunoprecipitation (IP). To do so we cloned cdhr1a
154 cDNA fused to a C-terminal FLAG tag into a mammalian expression vector and pcdh15b fused
155 to a C-terminal MYC tag. Using HEK293 cells we performed co-transfection and subsequently
156 FLAG and MYC pull down assays. Our results show that cdhr1a and pcdh15b can reciprocally
157 pull each other down in the IP assay (Fig 2A). While IP can indicate interaction between proteins
158 or between complexes of proteins, our hypothesis predicts that the interactions between cdhr1a
159 and pcdh15b are functional in that they connect the OS and CP in extracellular space. To test
160 whether cdhr1a and pcdh15b can form functional extracellular complexes we used the K562
161 leukemia cell line, which lacks any endogenous cadherin protein expression and therefore does
162 not form cell aggregates. Based on this fact, K562 cells are often used to test cadherin-cadherin
163 interactions [33]. As such, we transfected K562 cells with either cdhr1a-FLAG or pcdh15b-MYC to
164 test whether their interaction can result in K562 aggregation (Fig 2B). Introduction of either
165 cadherin alone resulted in minimal aggregation, either in total number of aggregates or the
166 number of cells per aggregate (Fig 2C-E). Conversely, when we mixed the cdhr1a-FLAG and
167 pcdh15-MYC expressing cultures we observed a significant increase in the total number of
168 aggregates and the number of cells in each aggregate (Fig 2C-E). Based on these results we
169 conclude that cdhr1a and pcdh15b can form cadherin-based junctions in extracellular space and
170 therefore have the potential to establish connections between the OS and CP in the retina.
171
172 **Generation of a zebrafish cdhr1a loss of function line for the study of cone-rod**
173 **dystrophy.**
174 CDHR1 deficiency has been modelled using the murine model which recapitulates the human
175 phenotypes associated with cone-rod dystrophy [34]. However, despite two decades since the
176 model was first generated, the mechanism behind PRC degeneration has yet to be elucidated.
177 While recapitulating the disease phenotypes, the mouse model does exhibit some limitations,

178 including having a rod-rich retina as well as the logistical difficulty in examining numerous
179 timepoints during early development, adolescence and throughout adulthood. As such, we
180 sought to model CDHR1-mediated cone-rod dystrophy using zebrafish which offers a vertebrate
181 cone-rich model that readily enables detailed molecular examination of PRCs at high temporal
182 resolution. Thanks to high conservation of ocular development, genetics and function, the
183 zebrafish model has been used to model numerous human ocular diseases including retinitis
184 pigmentosa, LCA, coloboma and numerous others.
185 Zebrafish encode two CDHR1 homologues, cdhr1a and cdhr1b, of which only cdhr1a is
186 expressed in the zebrafish photoreceptors [35]. We targeted cdhr1a using the Alt-R CRISPR
187 technology by designing two crRNA constructs separated by ~170bp and mapping to intron 6
188 and intron 7 (Fig 3A). Upon injection, we generated a stable zebrafish line harboring a 173bp
189 deletion which results in the excision of exon 6, and a premature stop codon at AA146 (Fig
190 3B,C). Cdhr1a protein sequence encodes 6 extracellular cadherin domains (EC1-6), a
191 transmembrane domain and a cytoplasmic domain (Fig 3D). The 173bp deletion is predicted to
192 result in a truncation of this polypeptide at AA146, therefore terminating the protein after just the
193 first EC domain. Thus, the remaining protein would lack both the transmembrane and
194 cytoplasmic domain and therefore would likely lose all function. The *cdhr1a*^{fs146*} line (from here
195 on referred to as *cdhr1a*$^{-/-}$) was bred to homozygosity to create a maternal zygotic mutant
196 population. The maternal zygotic mutants were used for all the subsequent functional
197 experiments. To confirm that our mutant line represented a null allele we probed for cdhr1a in
198 PRCs using a zebrafish specific cdhr1a antibody which we previously developed and verified [35].
199 As expected, immunohistochemistry (IHC) of 5 dpf wildtype zebrafish retinal cryosections
200 displayed strong cdhr1a staining at the inner/outer segment boundary in rod cells (Fig 3E).
201 However, cdhr1a$^{-/-}$ samples exhibited a total lack of cdhr1a protein signal, therefore confirming
202 that our mutant line harbors a null allele. Additionally, *in situ* hybridization data suggests that the
203 allele undergoes non-sense mediated decay and we do not detect any retinal expression of
204 cdhr1b as compensation (data not shown). Taken together we were able to generate a novel
205 zebrafish line harboring a heritable null allele in cdhr1a and establish a homozygous population
206 of fish suitable for functional analysis of PRC phenotypes throughout development, adolescence
207 and adulthood.
208
209 **Loss of cdhr1a function in zebrafish results in progressive cone-rod dystrophy.**

210 There are no studies to date that have examined effects of CDHR1 loss of function on CPs. As
211 such, to provide a more comprehensive examination of PRC phenotype progression we
212 examined 5 timepoints encompassing early development (5 and 15 dpf), juveniles (30 dpf) as
213 well as adults (90 and 180 dpf). At each timepoint we first examined the morphology and
214 number of cone cells as it is expected that these cells will be affected first. To visualize cone cell
215 OSs, we used a peripherin2 (prph2) antibody which labels the periphery of OSs in PRCs,
216 including all the cone subtypes. For consistency, we chose to sample all our timepoints at the
217 central retina (adjacent to the optic nerve). Starting at 5 dpf we observed that both WT and
218 cdhr1a$^{-/-}$ cone OSs exhibited their expected shape (Fig 4A, A') and displayed smooth vertical
219 peripheral prph2 staining. To determine whether there are any physiological changes to the
220 cone OS (COS) we also measured the OS length based on prph2 signal. When comparing WT
221 to cdhr1a$^{-/-}$ mutants we observed a slight, but significant increase in the average COS size from
222 4.79μm to 5.34μm (Fig 4F). At 15 dpf we again detected an increase in the average COS length
223 in the mutants from 6.74μm in WT to 7.95μm (Fig 4F). We also began to observe that the COS
224 shape appeared to become disorganized, perhaps due to the increase in length (Fig 4B,B').
225 Interestingly, by 30dpf, when the retina has been fully developed, we observed a significant
226 decrease in average COS length in the mutants, from 7.63μm in WT to 6.68μm (Fig 4F).
227 Additionally, the COS of the mutants continued to appear disorganized, lacking the smooth
228 vertical prph2 labeling observed in WT (Fig 4C) and instead displaying an almost disc like
229 organization (Fig 4C'). At 90 dpf there continued to be a decrease in average COS length
230 compared to WT, 8.40μm vs 6.81μm (Fig 4F) and increased OS disorganization. Furthermore,
231 at 90 dpf we noted a significant decrease in the number of cones suggesting that there was
232 degeneration of cone cells (Fig 4D, D', H). The most severe phenotype was observed at the
233 latest timepoint. At 180 dpf COS length further decreased to 4.84μm while the wildtype
234 remained at 8.62μm (Fig 4F). Furthermore, there was a striking reduction in the number of cone
235 cells remaining (Fig 4H) while COS morphology exhibited severely stunted and tilted COSs (Fig
236 4E'). Taken together, our examination of COS morphology, size and number of cone cells
237 indicates that in the absence of cdhr1a function cone cells lose normal OS morphology which
238 precedes their degeneration, which begins between one and three months.
239 In addition to fluorescence confocal microscopy analysis of OS morphology, we also examined
240 COSs at electron microscopy resolution using TEM. When comparing WT to cdhr1a mutants at
241 15 dpf we can already detect mis organization of the OS discs in the form of bulges and
242 improperly stacked discs (Fig 4Q-R). This result corresponds with our fluorescence microscopy

243 data (Fig 4B') where at 15 dpf we already see alteration in the pattern of prph2 staining. Taken
244 together, our data indicates that COS integrity is significantly affected by the loss of cdhr1a as
245 early as 15 dpf, and that this results in progressive loss of cone cells starting at 30 dpf and
246 proceeding up to and including 180 dpf (Fig 4G, H).
247 While cone cells were the primary target of our investigation of cone-rod dystrophy in our
248 cdhr1a$^{-/-}$ model, we also examined the fate of rod cells. Like our analysis of cones, we sought to
249 examine rod OS morphology, length and number of rod cells at the aforementioned timepoints.
250 Due to a delay in the assembly of the rod OSs (ROS) compared to COSs we used Gnb1
251 antibody (β subunit of rod specific transducin) to identify rod cells and wheat germ agglutinin
252 (WGA) to visualize their OS in early development (5 and 15 dpf), and subsequently prph2 and
253 WGA at later stages (30-180dpf). When analyzing both the morphology and length of ROSs we
254 observed that WT and cdhr1a$^{-/-}$ ROS were similar in appearance and number at early timepoints
255 (Fig 4I-J, P). Interestingly, like COSs, ROSs exhibited a slight increase in length, in the cdhr1a
256 mutants at 15dpf and 30dpf (Fig 4N). The first phenotypic difference for ROS was observed at
257 90dpf, where we detected a slight decrease in the average length, 26.6μm vs 30.3μm in WT
258 (Fig 1N). Furthermore we also noticed the first examples of morphological disorganization (Fig
259 4L, L') as well as a 3.4% decrease in the number of rod cells (Fig 4P). The trend of shorter ROS
260 and disorganized morphology continued up to 180dpf where the average OS length decreased
261 to 20.4μm vs 33.7μm for WT. Furthermore, at 180 dpf the number of rod cells decreased by
262 10%, likely stemming from the persistence of disorganized OSs leading to rod cell degeneration
263 (Fig 4P). Taken together, we conclude that rod cells are only marginally affected by the loss of
264 cdhr1a function in early development and early adulthood, and show significant phenotypic
265 effects starting at 180 dpf (Fig 4O, P). Based on our data, we predict that the molecular
266 mechanism driving cone-rod dystrophy in our mutant line is primarily involved in the
267 maintenance of COS homeostasis. Rod effects are either secondary responses to the loss of
268 cones or due to differences in the function of cdrh1a between rods and cones.
269
270 **Loss of cdhr1a function leads to CP disorganization.**
271 Since our hypothesis involves connections between OSs and CPs, we next examined the
272 consequence of cdhr1a function on CPs. Several previous studies have established that
273 zebrafish exhibit robust numbers of CPs whose assembly coincides with formation of the COSs
274 and ROSs [24,31]. To examine CP integrity, we measured their length and observed overall
275 morphology using actin antibody staining which is commonly used to assess CP size and

276 morphology [23,24,31,32]. To compare CPs between wildtype and cdhr1a$^{-/-}$ we measured their length
277 and observed their overall morphology. In line with previous results, we observed a gradual
278 increase in CP length in both cones and rods throughout early development (5-15 dpf) and a
279 steady state from adolescence to adulthood (30-180dpf) (Fig 5M, N). Furthermore, we observed
280 that zebrafish cone CPs are significantly longer, more than double, then their rod counterparts at
281 all time points analyzed. Longer cone CPs were previously also observed in macaque retina [23].
282 Next, we compared wildtype CPs to those of the cdhr1a$^{-/-}$ mutants. At 5 and 15 dpf we observed
283 that morphologically cone CPs in cdhr1a$^{-/-}$ resembled those of WT (Fig 1A-B'). However, even at
284 5 dpf measurements of CP length indicated a slight decrease in CP size in the mutants, 3.70μm
285 vs 3.49μm (Fig 5F) while at 15 dpf mutant CPs measured longer than wildtype, 5.54μm vs
286 6.72μm. Similar results were observed for rods where mutant CPs were longer at 15 dpf (Fig
287 5F-G'). Starting at 30dpf we began to observe not only morphological disorganization of actin
288 staining along CPs, but also a significant decrease in overall CP length in cdhr1a$^{-/-}$ samples (Fig
289 5C,C'). Cone CPs appear to have lost their tether to the OS and tilt away from the OS.
290 Interestingly, cdhr1a$^{-/-}$ rod CPs do not show any effects in their morphology or length at 30 dpf
291 (Fig 5H, H'). This trend continued and intensified in cone CPs at the 90 and 180 dpf timepoints
292 (Fig 5D-E',F). In fact, by 180 dpf we observed the length of cone CPs shorten to what it was at
293 5dpf, which is half of what WT exhibits at 180 dpf, 7.36μm vs 3.47μm (Fig 5E, E', F). For rod
294 CPs, we observed a much subtler effect, where the CP length isn't affected until 90dpf, and
295 even at 180 dpf the degree of decrease in size, 2.67μm vs 2.39μm, while significant was not
296 relatively as large compared to cone CPs (Fig 5I-J', G). Having noted significant effects on CP
297 size and morphology in the absence of cdhr1a function, we also examined for consequences on
298 pcdh15b localization. At 5dpf, cdhr1a$^{-/-}$ cone and rod cells displayed wildtype like localization of
299 pcdh15b (Fig 5O). However, pcdh15b localization in subsequent timepoints mirrored the
300 disorganization of the CP previously observed using actin (Fig 5A-J'). By 180 dpf, very little
301 pcdh15b signal remains (Fig 5J) suggesting a total degradation of CPs. Based on our actin CP
302 staining as well as pcdh15b signal, we conclude that the absence of cdhr1a does not affect the
303 assembly of the CP nor localization of pcdh15b to the CP, but does contribute to progressive
304 disorganization and degeneration of the CP, likely due to absence of connections with the OS.
305
306 **Pcdh15b is necessary for proper localization of cdhr1a.**
307 Recent studies in zebrafish have indicated that loss of pcdh15b results in malformation of OSs
308 and PRC degeneration [31]. To examine how the loss of pcdh15b compares to the loss of cdhr1a

309 we generated a CRISPR/cas9 knockout line by targeting two crRNAs in exon 5, which resulted
310 in a heritable 68bp deletion (Fig 6A). The consequence of the deletion was a frame shift at
311 AA117 and a premature stop at AA118. Like our *cdhr1a*^{fs*146} allele, the *pcdh15b*^{fs117*118} allele
312 (subsequently referred to as pcdh15b$^{-/-}$) results in a truncation of the protein before either the
313 transmembrane domain or the cytoplasmic domain, thus likely representing a null. To confirm
314 the null phenotype, we probed for pcdh15b in retinal cryosections using IHC and observed a
315 lack of pcdh15b signal in pcdh15b$^{-/-}$ samples, validating the allele as a null (Fig 6B-B"). Due to
316 critical function of pcdh15b in the inner ear, pcdh15b$^{-/-}$ larva were only viable up to
317 approximately 10 dpf, an outcome previously reported in zebrafish [31]. To observe the effects of
318 pcdh15b loss of function on PRCs we first analyzed cone OS morphology and size. Due to the
319 immaturity of rods at 5 and 10 dpf and cone specific effects observed in the cdhr1a$^{-/-}$ mutant, we
320 focused our attention to cone cells. Using prph2 staining we observed little effect on COS
321 morphology or length at 5dpf (Fig 6C-C"). However, at 10 dpf pcdh15b$^{-/-}$ COSs displayed
322 disorganization and a slight decrease in COS length (Fig6 D-D", E). Next, we examined CP
323 morphology, where at 5 dpf CP morphology in mutants resembled that of wildtype (Fig6 F-F"),
324 however, by 10 dpf mutant CPs showed signs of disorganization (Fig 6G-G"). Quantification of
325 CP length at 5 dpf pcdh15b$^{-/-}$ larva revealed a slight, yet significant increase in CP length
326 although by 10dpf no difference in CP length between wildtype and mutant was detected (Fig
327 6H). Lastly, we examined whether loss of pcdh15b had any effects on cdhr1a localization. To
328 quantify we measured the length of cdhr1a signal along the OS. In doing so we observed that
329 loss of pcdh15b did not preclude cdhr1a from localizing to OS, however as early as 5dpf
330 pcdh15b mutants display a significant decrease in the spread of cdhr1a signal along the OS (Fig
331 6I-I"), which became much more pronounced by 10 dpf (Fig 6J-J"). Quantification of cdhr1a
332 signal length along the OS revealed a significant decrease as early as 5 dpf, 3.22μm vs 2.59μm,
333 and a major decrease by 10 dpf, 4.06μm vs 1.64μm (Fig 6K). Taken together we conclude that
334 while pcdh15b is not required for cdhr1a localization to the OS, spread of cdhr1a signal along
335 the cone OS, which likely represents OS-CP interactions, requires pcdh15b.
336
337 **Loss of cdhr1a and pcdh15b synergize resulting in severe CP disruption and cone outer**
338 **segment malformation.**
339 Having observed phenotypes affecting CPs and OSs in both cdhr1a and pchd15b individual
340 mutant lines, we next asked whether a combination of both mutations would lead to more
341 severe outcomes. To do so, we established a *cdhr1a*$^{-/-}$ *; pcdh15b*$^{+/-}$ line. By crossing this line we

342 were able to collect 5 and 10dpf embryos that lacked both cdhr1a and pcdh15b (cdhr1a$^{-/-}$;
343 pcdh15b$^{-/-}$) function. We then again performed our morphological analysis of cone OSs using
344 prph2 antibody staining and CPs using actin antibody staining. At 5 dpf we observed little
345 change in COS morphology when comparing cdhr1a$^{-/-}$ to pchd15b$^{-/-}$ mutants (Fig 7A,B). COS
346 length however differed, where cdhr1a$^{-/-}$ individuals display significantly longer COSs at 5.63μm
347 versus 4.96 for pcdh15b$^{-/-.}$ Interestingly, when comparing the double mutant to either single
348 mutant, or any of the other genetic combinations we observed a significant decrease in COS
349 length, 3.68μm, as well as disorganized COS morphology (Fig 7A-D). This trend was even more
350 pronounced at the 10 dpf timepoint, where disorganization of the COS was highly evident in the
351 double mutant (Fig 7E-H). Furthermore, the double mutant COS length decreased to 4.31μm
352 compared to 7.83μm for cdhr1a$^{-/-}$ and 6.31μm for pcdh15b$^{-/-}$ (Fig7 E-I). Thus, it appears that
353 concurrent loss of cdhr1a and pcdh15b combines to result in significant decreases in COS
354 length as well as very early morphological COS disorganization.
355 When examining CP length and morphology we observed similar trends. At 5 dpf, cdhr1a
356 mutants exhibit elongated CPs with normal morphology, compared to slightly truncated but
357 morphologically normal CPs in pcdh15b mutants (Fig 7K,L). Double mutants display normal CP
358 morphology at 5 dpf, albeit their CPs are significantly shorter than wildtype (3.22μm vs 2.45 μm)
359 (Fig 7N, S). By 10 dpf both CP morphology and length are significantly affected in the double
360 mutant compared to either single mutant (Fig 7O-P, T). CPs appear severely disorganized
361 lacking the expected vertical actin staining, instead appearing shorter and bent or tilted. When
362 comparing CP lengths, the double mutant has severely truncated CPs, 2.93μm vs 6.34μm in
363 cdhr1a mutants and 5.82μm in pcdh15b mutants. Taken together, we conclude that the
364 combination of pcdh15b and cdhr1a loss of function enhances both COS disorganization and
365 decreases COS length along with CP morphological disruption and severe truncation even at
366 very early timepoints. These findings further support our hypothesis where cdhr1a functions to
367 link cone OSs with CPs by interacting with pcdh15b.
368
369
370 **DISCUSSION**
371 Discovered over 20 years ago, the retinal cadherin CDHR1 is clinically associated with
372 recessive cone-rod dystrophy, yet its exact molecular function continues to remain a mystery. In
373 our current study we found that the zebrafish homologue of CDHR1, cdhr1a, localizes to cone
374 and rod OSs in a pattern mirroring that of the inner segment calyceal processes and its own

375 resident cadherin pchd15b (PCDH15 homolog in zebrafish). Interestingly, the pattern of
376 CDHR1/PCDH15 localization was observed across various species, including amphibians,
377 rodents, birds, primates and humans, thus indicating a high degree of mechanistic evolutionary
378 conservation. Aquatic species, zebrafish and xenopus, appear to have retained significant
379 length of their cone CPs, particularly along the UV cones, as evident by the length of
380 cdhr1/pcdh15 signal (Fig 1C, E). Conversely in rodents, which have been previously shown to
381 exhibit the shortest CPs, CDHR1/PCDH15 juxtaposition is still maintained albeit in a very short
382 segment [23]. Intriguingly, the size of the CP may be related to the diurnal nature of an organism
383 as the gerbil exhibited much longer CPs compared to rats and mice (Fig 1G-J). Birds and
384 primates exhibit CP lengths longer than rodents but still shorter than fish or frogs (Fig 1K-L). In
385 addition to localization, we showed that cdhr1a physically interacts with pcdh15b *in vitro,* via co-
386 immunoprecipitation and *in vivo* via the K562 cell aggregation assay (Fig 2). Importantly, the
387 localization and interaction findings provide the first potential clue as to the molecular function of
388 CDHR1 and the etiology of CDHR1-associated cone-rod dystrophy. Based on these findings we
389 hypothesize that cdhr1a links the OSs with the CPs via interactions with pcdh15b and postulate
390 the absence of this interaction as a mechanism driving cone cell degeneration.
391
392 To test our hypothesis, we tracked cone-rod dystrophy progression in zebrafish using single
393 cdhr1a$^{-/-}$ or pcdh15b$^{-/-}$ mutant lines as well as a cdhr1a$^{-/-}$, pcdh15b$^{-/-}$ double mutants. Taking
394 advantage of the zebrafish system we were able to examine CRD progression at numerous
395 developmental and adult stages at the molecular level with high resolution. When examining the
396 cdhr1a$^{-/-}$ model, we documented progressive disorganization and shortening of cone OS starting
397 at 30 dpf, while observing only minor effects in rods (Fig 4). Interestingly, disorganization and
398 shortening of cone OSs at 30 dpf was preceded by slight but significant lengthening at 10 dpf.
399 This suggests that early development of the OS may be regulated by CP-OS interactions to
400 ensure proper rate of OS growth (Fig 4G). Cdhr1a$^{-/-}$ cones exhibited shortened and disorganized
401 CPs as early as 15dpf, indicating that defects in CP-OS interactions precede and may therefore
402 lead to cone OS instability. A striking phenotype observed in mutant cone OSs was the mis
403 organization of prph2 signal. Normally prph2 signal appears smoothly along the periphery of
404 cone OS and largely absent from the center, however, in cdhr1a$^{-/-}$ cones we observe an almost
405 disc like horizontal staining of prph2 throughout the OS as early as 15 dpf and very clearly by
406 30dpf (Fig 4B'-E'). Prph2 mis organization was also accompanied by the appearance of cone
407 OS bending and tilting, compared to wildtype (Fig 4A-E'). Similar prph2 localization phenotypes

408 have been observed in prom1b mutant zebrafish, which is interesting as prom1 has been shown
409 to interact with Cdhr1 [15]. Perhaps loss of prom1b results in the mis-localization or mis-regulation
410 of cdhr1a in the cone OS and therefore also compromises CP-OS interactions leading to similar
411 phenotypes. Finally, using TEM, we observed that cdhr1a$^{-/-}$ cone OSs displayed disorganized
412 disc stacking, which supports the observed prph2 localization phenotype (Fig 4Q-R). Several
413 previous studies have postulated that CP-OS interactions are critical for stability of cone OSs
414 [23,24,32]. Our data supports this notion where cdhr1a mutant cone OSs are shorter and often
415 appear tilted to one side. Similar OS phenotype results were also observed in pcdh15b mutants
416 up to 10dpf which is in line with previous reports from zebrafish and what was also observed in
417 xenopus embryos injected with Pcdh15 morpholinos [31,32]. Pcdh15b mutants display cone OS
418 defects earlier than cdhr1a$^{-/-}$ and do not exhibit the early increase in OS length. This might
419 suggest that the absence of pcdh15b interferes with CP function, while the absence of cdhr1a
420 interferes with OS-CP connections but not the CP itself. In the double mutants, absent of both
421 cadherins, we observed shorter and disorganized CPs and cone OSs as early as 5 dpf, normally
422 not seen in either single mutant alone (Fig 7 I,J,S,T). By 10 dpf the double mutant phenotypes
423 were severe and comparable to what we observed in cdhr1a$^{-/-}$ mutants by 30+ dpf (Fig 4C'-E',
424 7H). The exacerbation of phenotypes in the double mutant further supports our model where
425 cdhr1a and pchd15b function to anchor cone OSs with CPs. Interestingly, these results also
426 suggest that in the absence of either cdhr1a or pchd15b there may be redundant mechanisms
427 that aid in OS-CP anchoring. Perhaps other retinal cadherins can interact with cdhr1a or
428 pcdh15b, albeit not as strongly or efficiently, and delay the early phenotypes until the OS are
429 fully mature. Taken together, our data along with previous studies strongly supports the
430 hypothesis that in the absence of cdhr1a function the CP-OS interaction is compromised and
431 thus hampers cone OS integrity.
432
433 While the focus of our study was on cone cells, we also characterized effects of cdhr1a loss
434 on rods. Rod OSs, nor their CPs appear to be significantly affected by the loss of cdhr1a
435 function until later stages, 3 months or longer (Fig 4 N-P). Albeit significant, these effects were
436 much less obvious compared to the effects on cones, as one might expect for a cone-rod
437 dystrophy model. Furthermore, while cone CPs displayed gross morphological defects, rod CPs
438 were only slightly affected even at later timepoints (Fig 4M'). This likely stems from the fact that
439 rod CPs are inherently much smaller than cone CPs and may not serve as critical a role in rods
440 as we predict they do in cones. Comparing rod CP length over the course of development and

441 adulthood in our study we note that rod CPs are on average approximately one third the size of
442 cone CPs (Fig 5M-N). Furthermore, compared to the length of rod OS, rod CPs encompass a
443 very small portion of the OS, while in cones CPs extend up to three quarters of the cone OS
444 length. Based on work in the murine model and our own observations of rod CPs, we
445 hypothesize that zebrafish rod CPs only extend along the newly forming OS discs and do not
446 provide structural support to the ROS. As such, we support the hypothesis postulated by
447 Burgyone 2015 *et al* that in rods, Cdhr1a functions to anchor newly formed OS discs to facilitate
448 proper maturation of the discs prior to release into the OS. While this differs from its function in
449 cones, cdhr1a still likely relies on its interaction with pcdh15b to serve this function as the two
450 proteins clearly juxtapose in rod cells across all the species we examined, including rodents
451 which have been hypothesized to lack CPs or have very simplified versions of CPs compared to
452 other species [23].
453
454 Discovery of the interaction between cdhr1a and pcdh15b is novel. Previous studies have
455 suggested that PCDH15 and CDH23 are binding partners in the retina as they are well known to
456 interact in the inner ear stereo cilia [32]. However, our work, and others, have shown that cdh23 is
457 not expressed in zebrafish retina nor does loss of cdh23 result in ocular phenotypes (Fig S1).
458 Work from macaque retina shows cdh23 expression in the OS/IS region but does not display the
459 prototypical CP staining as observed with pcdh15 or actin [23]. While several Usher 1 proteins
460 other than pcdh15 have been found to localize to the CP, including harmonin, myosin and sans,
461 there has been a missing link between pcdh15 in CP and its potential partner the OS, which we
462 now propose to be Cdhr1. In our study, cdhr1a-pcdh15b interactions are supported by
463 immunoprecipitation and cell aggregation assays and by the fact both are cadherin proteins that
464 can facilitate heterophilic interactions (Fig 2). PCDH15 is known to generate cis dimers like
465 cdh23, and as such the cdhr1a-pcdh15b interaction may in fact involve tetrameric complexes [36].
466 Additional evidence for the cdhr1a-pcdh15b interaction was the observation that cdhr1a
467 localization along the cone OS was significantly impaired in the absence of pcdh15b function. At
468 5 dpf and even more so at 10dpf the length of cdhr1a signal along the cone OS was severely
469 reduced, while cone OS length was only slightly affected (Fig 6 I-J”). Thus, we conclude that
470 while pcdh15b is not necessary for cdhr1a to localize to the base of cone OSs, its absence
471 prevents cdhr1a from forming connections to the CP and subsequently extending along the
472 length of the OS. Other proteins may further regulate cdhr1a-pcdh15b complexes such as
473 prom1b, which is known to interact with cdhr1, as well as other Usher 1 proteins found in the

474 CP. CDHR1 is also known to undergo proteolytic cleavage to remove its extracellular cadherin
475 domains, which could further regulate the interaction and stability of the CP-OS attachments [9]. It
476 remains unclear if the cleavage occurs in both rod and cone cells. We hypothesize that
477 proteolytic cleavage is specific to rods, where this would aid in regulating the release of the
478 newly matured OS discs, while cleavage would be absent in cone cells as to ensure CP-
479 mediated OS structure and integrity. Interestingly, we have also previously reported that cdhr1a
480 can be targeted by the Siah1 ubiquitin ligase for proteasomal degradation, adding yet another
481 layer to the potential complexity of regulating cdhr1a [37]. Imaging of siah1 indicates that it also
482 localizes to the OS in a pattern similar to that of cdhr1a (data not shown). Future studies will be
483 required to elucidate the entire complex responsible for the anchoring and maintaining of CPs
484 and OSs in rods versus cones.
485
486 Overall, our cdhr1a$^{-/-}$ model corroborates findings from the mouse CDHR1 KO model with
487 early phenotypes found exclusively in cone cells, and only at later stages, 6+ months, displaying
488 rod cell OS disorganization and degeneration. In conclusion, we propose that cdhr1a and
489 pcdh15b function to link the cone OS and the CP to maintain cone homeostasis in an
490 evolutionarily conserved manner. Disruption of this interaction may therefore be a potential
491 driving factor in the progression of cone-rod dystrophy observed in CDHR1 patients. Future
492 studies will need to focus on the molecular consequences of OS-CP interaction and the identity
493 of the entire repertoire proteins involved as well as any potential signaling pathways that
494 activate in response to sensing or monitoring OS-CP interactions.

495 **MATERIALS & METHODS**

496

497 Zebrafish Husbandry and Embryo maintenance

498 Zebrafish husbandry used in all procedures were approved by the University of Kentucky
499 Biosafety office as well as IACUC Policies, Procedures, and Guidelines and ethical standards.
500 The AB strain was used as wildtype. ALT-R-CRISPR Cas9-based mutant lines were generated
501 based on protocols established previously [35]. Embryos were kept at 28°C in E3 embryo media.
502 At indicated times in the study, embryos and adults were euthanized by cold shock or in tricaine
503 before harvesting the eyes and fixation with 4% PFA in PBS overnight at 4°C.

504

505 Statistical analysis

506 All the data sets were analyzed using Prizm 8. Data shown on graphs represents individual
507 measurements +/- standard deviation. Each of the data points had an n of 5+ individuals.
508 Student's t-test was used to analyze direct comparison between ages or genotypes while
509 ANOVA was used to assess significance of the entire data set.

510

511 Availability of data and materials.

512 All data generated or analyzed during this study are included in this published article. All
513 materials, zebrafish lines, and reagents will be shared upon request after publication.

514

515 Whole mount In Situ Hybridization

516 WISH was performed as previously described [38]. RNA probes were generated via PCR
517 amplification from 3 dpf cDNA fused to T7 promoter sequence and subsequently transcribed
518 (DIG or FITC labeled) using T7 polymerase (Roche). Primer sequences can be found in
519 supplemental table 1. Approximately 1000bp was amplified from the 3' end of each cDNA. WISH
520 was performed as previously described [38]. Images were captured using a Nikon Digital sight DS-
521 U3 camera and Elements software. Image adjustment was performed using Adobe Photoshop.

522

523 Cryosection and Immunofluorescence/IHC

524 Embryos and adult eyes were fixed in 4% paraformaldehyde then washed out PBS with
525 0.1%Tween-20. Next, the specimens were washed overnight in 10% then 30% sucrose
526 overnight at 4°C. Transverse, 10 mm sections were collected, beginning just anterior to and
527 ending posterior to the eye. For imaging and cell quantification, only the sections containing the

528 lens were used for consistency. Immunofluorescence was performed as described previously
529 with addition of a Tris-EDTA based antigen retrieval step prior to serum blocking the specimen
530 [35]. Post blocking, following antibodies and lectins were used: anti-zcdhr1a (Cdhr1a, rabbit,
531 1:100, SKU:DZ07988 Boster Bio, Pleasonton, CA, United States), anti-hcdhr1 (CDHR1, rabbit,
532 1:100, PA5-57832 Thermo Fisher, Waltham, MA, United States), anti-hpcdh15 (Pcdh15, sheep,
533 1:75, PA5-47865 Thermo Fisher, Waltham, MA, United States), anti-prph2 (Peripherin – 2,
534 rabbit, 1:100, 18109-1-AP Protein-tech, Rosemont, IL, United States), anti-actin (beta Actin,
535 mouse, 1:100, MA1-140 Thermo Fisher, Waltham, MA, United States) anti-gnb1 (GNB1, rabbit,
536 1:100, PA5-30046 Thermo Fisher, Waltham, MA, United States), anti-zrhodopsin (1d1 epitope of
537 the zebrafish rhodopsin, mouse 1:100, Fadool lab, Florida State University, FL, United States).
538 Alexa fluor 488, 555, and 647 conjugated secondary antibodies at a concentration of 1:200
539 (Thermo Fisher, Waltham, MA, United States) were used with DAPI as a counter stain. Further,
540 Lectins: Peanut Germ Agglutinin conjugated with a 488 fluorophore (1:100 concentration,
541 #29060 Biotium, San Francisco, CA, United States) and Wheat Germ Agglutinin conjugated with
542 a 405 fluorophore (1:50 concentration, #29028-1 Biotium, San Francisco, CA, United States)
543 were used to label PRC outer segments.
544
545 Confocal/SIM imaging
546 For Immunofluorescence, slides were mounted in Vectashield antifade mounting medium (H-
547 1700-10 Vector laboratories, Newark, CA, United States) then imaged on a Nikon C2 confocal
548 microscope under a 60X 1.4 NA oil immersion objective. For consistency all the images were
549 captured from the central retina to assess all the major types of photoreceptors. Super
550 resolution microscopy was performed on a Nikon A1R confocal microscope equipped with a
551 Structured Illumination Microscopy module and a CMOS sensor under a 100X 1.49 NA oil
552 immersion objective. Quantification of OS length and number was performed using confocal
553 captured images in Image J.
554
555 Cloning
556 A previously developed and verified Cdhr1a mammalian cell expression plasmid of Cdhr1a
557 tagged with FLAG in pCIG2 developed via Infusion HD cloning plus (Takara) was used in this
558 study [35]. To develop an expression construct for Pcdh15b, we amplified pcdh15b cDNA from
559 3dpf WT embryos (5'CATCATGATATCACCATGAAGATGCGCCAGAGGTCG-
560 3', 5'ATGATGTTCGAACAGAACAGTGGACTGAGATGG3') and cloned into the Topo XL vector

561 (Invitrogen). Subsequently we directionally cloned pcdh15b cDNA into the pCDNA3-MYC
562 expression plasmid using Kpn1 and Xho1. Both constructs were verified using sanger
563 sequencing (Eurofinsgenomics).
564
565 Immunoprecipitation
566 For transient mammalian cell transfection a previously established protocol was used with slight
567 modifications [39]. First, HEK 293 cells were cultured at 37 °C in DMEM media until 70%
568 confluency. Next, aforementioned plasmids individually or in combinations of Cdhr1a:FLAG
569 pCIG2 (1ug) and Pcdh15b:MYC pCDNA (1ug) were first incubated with PEI (polyethyleneimine)
570 at room temperature for 30 mins. Upon HEK 293 cell confluency, these PEI/DNA complexes
571 were transfected to the cells and incubated at 37°C for 24 hours. Protein extraction was
572 performed based on the Mem-PER plus extraction protocol (#89842 Thermo Fisher). To inhibit
573 protease activity, we added HALT protease inhibitor (1:1000 #78425 Thermo Fisher). For co-
574 immunoprecipitation (co-IP), one Cdhr1a and Pcdh15b cotransfected protein sample was
575 incubated with Anti-FLAG magnetic beads (A36797 Thermo Fisher) while another cotransfected
576 sample was incubated with Anti-MYC magnetic beads (#88842 Thermo Fisher). For IP control,
577 Cdhr1a-FLAG transfection samples were immunoprecipitated (IP) using Anti-MYC beads while
578 Pcdh15b-MYC transfection samples were immunoprecipitated using Anti-FLAG beads. Next, all
579 the lysate control, control IP, and co-IP samples were prepared with 6X SDS sample buffer
580 under reducing conditions and boiled at 96°C for 7 mins. Samples were then ran in two 7.5%
581 SDS PAGE gels at 140 volts for 90 mins. They were then transferred to a PVDF membrane for
582 90 mins at 20 volts. The membranes was then blocked with 1X Blocker™ (#37565 Thermo
583 Fisher) for 1 hour at room temperature. Next, one membrane was probed for FLAG via mouse
584 Anti-FLAG (1:1000 F1804 Sigma Aldrich, St. Louis, MO, United States) and the other membrane
585 was probed for MYC via mouse Anti-MYC (1:1000 MA121316 Thermo Fisher). These primary
586 antibodies were incubated after blocking at 4°C overnight. The following day membranes were
587 washed 3 times with TBS (5 mins each). Subsequently, the membranes were incubated with
588 goat anti-mouse secondary antibody conjugated with poly HRP at 1:2000 concentration in the
589 1X Blocker™ for 1 hour at room temperature. Next, the membranes were again washed with
590 TBS buffer for 3 times (5 mins each). To detect the HRP signal, SuperSignal™ West Pico PLUS
591 Chemiluminescent Substrate (#34580 Thermo Fisher) was used and chemiluminescence
592 images were then detected and captured using Amersham Imager 680.
593

K562 assay

For the cell aggregation assay, K562 cells were cultured at 37°C in RPMI 1640 media until 70% confluency. Cdhr1a and Pcdh15b expression plasmids were incubated with the PLUS reagent for 15 mins in the same RPMI 1640 media and then Lipofectamine LTX was added and incubated for 25 mins at room temperature to form Lipofectamine-DNA complexes. The complexes were then transferred to the cells and incubated at 37°C for 24 hours. Next day individual transfections of Cdhr1a and Pcdh15b were cocultured by gently mixing and rocking the cells back and forth allowing the aggregates to form. K562 cell aggregates were then imaged on EVOS FLoid cell culture microscope (#4471136 Thermo Fisher).

TEM

TEM sample preparation was slightly modified from *Miles et al.* 2021. First, zebrafish larvae and adult specimens were fixed in 2.5% glutaraldehyde and 2% paraformaldehyde in 0.1M phosphate buffer at 4°C overnight on a shaker. Samples were then washed 5 times with 0.1M phosphate buffer (with 0.1% Tween-20) for 5 times - 10 minutes each to wash out the aldehyde fixatives. Next, samples were placed in 1% Osmium tetroxide solution for 1.5 hours in dark at room temperature on a shaker. Samples were then washed again with 0.1M phosphate buffer with Tween-20 for 5 times – 5 minutes each and subsequently dehydrated with a series of ethanol washes at 50% (10mins), 70% (10 mins), 80% (10 mins), 90% (15 mins), and two 100% ethanol washes (15 mins each). Next, the specimens were infiltrated with LR white resin through a series of ethanol:resin combinations 25% LR white:75% ethanol (30 mins), 50% LR white:50%ethanol (30 mins), 75% LR white:25% ethanol (1 hour), and with 100% LR white (overnight at 4°C). The following day samples were exchanged with fresh 100% LR white for 3 hours and then samples were placed in “00” gelatin capsules or sealed PCR tubes in order to perform anaerobic polymerization required for LR white at 65°C. One micron thin sections were collected via a glass blade from the resin blocks using Leica EM UC7 and were stained with Toluidine blue to assess the location of samples being sectioned. Once satisfied with the location, ultrathin 70nm sections were collected using a diamond knife (Ultra 45° DiATOME, Quakertown, PA, United States) and placed on slotted EM grids (G2010-Ni Electron Microscopy sciences, Hatfield, PA, United States) covered in a layer of 0.5% formvar. Sections were then stained with a non-radioactive heavy metal UranyLess EM stain (#22409 Electron Microscopy sciences) for 1 hour followed by Reynold’s lead citrate stain for 30 mins. Images were then collected using FEI Talos F200X at 200 keV.

627

628 CRISPR

629 To establish the CRISPR/Cas9 based mutant lines, we ordered predesigned and synthesized
630 ALT-R Crispr crRNA (IDTDNA) targeting Cdhr1a (GTCTGGAAGTAGCATCTATA,
631 TCTGGCACATCTACGATGGA and Pcdh15b (CACCACAATGGACTGGATGT,
632 CGACTATCCGCACCTCGTGT). Next crRNA-tracrRNA duplexes were constructed before
633 injecting with Alt-R Cas9 v.3 enzyme in single cell staged embryos as described previously [40].
634 Genotyping was performed by designing primer oligos upstream and downstream of the
635 expected CRISPR/Cas9 based deletion sites and the resulting difference in sequence size was
636 used to genotype using DNA gel electrophoresis. (Cdhr1a: 5'-GTGTTAAAATTTGAATGCTGAG-
637 3', 5'-CTGCATATGCTTAGATGTTACC-3' ,pcdh15b: 5'-GAAACACAAAAGAAGCTGCG-3',
638 5'- GCCTTTATAATGGAGCGCAAG-3') Both Cdhr1a and Pcdh15b deletion sequences were
639 then confirmed via Sanger sequencing after outcrossing for two filial generations.

640

641 Competing interests

642 The authors declare that they have no competing interests.

643

644 Author contributions

645 JKF and MP designed the experiments. JKF and MKP wrote and edited the manuscript.
646 Experiments were carried out by MKP and WP.

647

648 **ACKNOWLEDGEMENTS**

649 We thank Dr. Ann Morris for insightful comments and review of the manuscript. Thanks to Dr
650 C.T Lutz for providing the K562 cells and Dr. Chintan Kikani for providing HEK293 cells and
651 tissue culture facilities. TEM work was done at the UKY EM facility, and we thank Jillian Cramer
652 and Dr. Nicolas Briot for technical assistance. SIM was performed at the UKY Light microscopy
653 core, and we thank Dr. Xu Fu for technical assistance.

654

655 **FUNDING**

656 This work was supported by a grant from the Retina Research Foundation awarded to JKF
657 and the Gertrude Ribble Pilot Grant awarded to MP.

658

659

660 **FIGURE LEGENDS**

661 **Figure 1:** Evolutionarily conserved localization of pcdh15 and cdhr1 in photoreceptors predicts
662 interactions linking outer segments and calyceal processes.
663
664 **A-A")** Confocal microscopy of wildtype 5dpf retinal cryosections probed with cdhr1a antibody
665 (green), Peanut germ agglutinin (PNA - magenta), Wheat germ agglutinin (WG - teal) and
666 pcdh15b (red). White boxes indicate the location of the inset enlargement. White arrowheads
667 highlight the linear localization of cdhr1a along cone OSs (A) and pcdh15b outlining the calyceal
668 process (A'). Merge of all three signals highlights the proximity between cdhr1a and pcdh15b
669 (A"). Scale bar = 10μm. **B)** Confocal microscopy of wildtype 5dpf retinal cryosections probed
670 with cdhr1a antibody (green), pcdh15b (red) and WGA (teal). White boxes indicate the location
671 of the inset enlargement. White arrowheads highlight the linear localization of cdhr1a along rod
672 OSs (B) and pcdh15b outlining the calyceal process (B'). Merge of all three signals highlights
673 the proximity between cdhr1a and pcdh15b (B"). Scale bar = 10μm. **C)** Structured illumination
674 microscopy (SIM) of wildtype zebrafish retinal cryosections probed with cdhr1a (green) and
675 pcdh15b (red). White box represents the inset enlargement. White arrowheads highlight the
676 juxtaposition of the cdhr1a and pcdh15b signals. Scale bar = 10μm. **D)** Diagrammatic model of
677 the connection between the OS discs and CPs in both rod and cone cells mediated by the
678 interaction between OS bound cdhr1a and CP bound pcdh15b. **E-L)** Structured illumination
679 microscopy (SIM) of wildtype xenopus (E), mallard duck (F), mouse (G), rat (H), spiny mouse (I),
680 gerbil (J), macaque (K) and human (L) retinal sections probed for cdhr1 (green) and pcdh15
681 (red). White boxes represent the inset enlargements. White arrowheads highlight the
682 juxtaposition of the cdhr1a and pchd15b signals in each species. The model figure was
683 prepared using Biorender. Scale bar = 10μm.
684
685 **Figure 2:** Physical interactions between cdhr1a and pchd15b can facilitate cell-cell adhesion.
686
687 **A)** Immunoprecipitation of cdhr1a-FLAG and pcdh15b-MYC performed in HEK293 cell lysates.
688 Pull down of cdhr1a-FLAG using anti-FLAG antibody beads also pulls down pcdh15b-MYC,
689 while pull down of pcdh15b-MYC using anti-MYC antibody beads also pulls down cdhr1a-FLAG.
690 **B)** Diagrammatic representation of the K562 cell assay for assessing homophilic or heterophilic
691 interactions between cadherins. **C)** Brightfield microscopy analysis of K562 cell aggregation
692 after transfection with either cdhr1a or pcdh15b or after co-culture of the two transfected
693 populations. Magenta boxes indicate regions enlarged in the insets. **D)** Quantification of the total
694 number of aggregates observed in a single field of view. **E)** Quantification of the number of
695 average number of cells in each observed aggregate.
696
697
698 **Figure 3:** Construction and confirmation of the cdhr1a$^{-/-}$ line.
699
700 **A)** Exon/intron diagram of cdhr1a. The intron 6-exon 6-intron 7 junction is highlighted and the
701 approximate location of the crRNA (black arrows) is depicted. **B)** Genomic nucleotide sequence
702 from the cdhr1a$^{\Delta 173}$ line highlighting the sequence location of the 173 bp deletion compared to
703 WT sequence. **C)** Amino acid sequence alignment between wildtype and the cdhr1a$^{\Delta 173}$ line.
704 Alignment indicates that the 173bp deletion leads to a frameshift and an immediate premature
705 stop codon at AA146. **D)** Diagrammatic representation of the domain structure of WT cdhr1a
706 protein vs the cdhr1a$^{\Delta 173}$ allele. EC = cadherin domain, TD = transmembrane domain, CD =
707 cytoplasmic domain. **E)** Confocal microscopy of 5 dpf retinal cryosections from WT and cdhr1a$^{-/-}$
708 retinas stained with anti-cdhr1a antibody (magenta), anti-rhodopsin antibody (green) and DAPI

(blue). Cdhr1a signal is clearly labelled at the ROS/RIS boundary in the wildtype and completely missing in cdhr1a$^{-/-}$. ROS = rod outer segment, RIS = rod inner segment. Scale bar = 10μm.

Figure 4: Loss of cdhr1a function leads to cone-rod dystrophy.

A-E) Confocal microscopy of wildtype retinal cryosections probed with anti-prph2 antibody (green). Scale bar = 10μm. **A'-E')** Confocal microscopy of cdhr1a$^{-/-}$ retinal cryosections probed with anti-prph2 antibody (green). Scale bar = 10μm. **F)** Quantification of cone OS length at 5, 15, 30, 90 and 180 dpf measured as length of prhp2 signal in wildtype (black dots) and cdhr1a$^{-/-}$ (blue dots). Standard deviation is shown in red. **** = $p<0.0001$. ANOVA = $p<0.0001$. **G)** Line graph depicting the long-term trend of cone OS length changes between wildtype (black) and cdhr1a$^{-/-}$ (blue). **H)** Line graph depicting changes in the number of cone cells counted in the observation region over time in wildtype (black) compared to cdhr1a (blue). **I-J)** Confocal microscopy of wildtype retinal cryosections probed with Gnb1 antibody (magenta) and WGA (teal) to identify rod outer segments. Scale bar = 10μm. **I'-J')** Confocal microscopy of cdhr1a$^{-/-}$ retinal cryosections probed with Gnb1 antibody (magenta) and WGA (teal) to identify rod outer segments. Scale bar = 10μm. **K-M)** Confocal microscopy of wildtype retinal cryosections probed with prph2 antibody (magenta) and WGA (teal) to identify rod outer segments. Scale bar = 10μm. **K'-M')** Confocal microscopy of cdhr1a$^{-/-}$ retinal cryosections probed with prph2 antibody (magenta) and WGA (teal) to identify rod outer segments. Scale bar = 10μm. **N)** Quantification of rod OS length at 5, 15, 30, 90 and 180 dpf measured as length of WGA signal in wildtype (black dots) and cdhr1a$^{-/-}$ (blue dots). Standard deviation is shown in red. ** = $p<0.001$, **** = $p<0.0001$. ANOVA = $p<0.0001$. **O)** Line graph depicting the long-term trend of rod OS length changes between wildtype (black) and chdr1a$^{-/-}$ (blue). **P)** Line graph depicting changes in the number of rod cells counted in the observation region over time in wildtype (black) compared to cdhr1a$^{-/-}$ (blue). **Q)** Transmission electron microscopy micrographs from a 15dpf wildtype retina. Yellow rectangle represents the enlarged inset. Magenta arrow heads highlight the proper stacking of OS discs. IS= inner segment, OS = outer segment. Scale bar = 500nm. **R)** Transmission electron microscopy micrographs from a 15dpf cdhr1a-/- retina. Yellow rectangle represents the enlarged inset. Magenta arrow heads highlight the improper and distorted stacking of OS discs. IS= inner segment, OS = outer segment. Scale bar = 500nm.

Figure 5: Calyceal processes in cones are disorganized in the absence of cdhr1a function.

A-E) Confocal microscopy of wildtype retinal cryosections probed with actin-antibodies (white) at various timepoints detecting cone CPs. Typical length of CPs observed is demonstrated in magenta. Scale bar = 10μm. **A'-E')** Confocal microscopy of cdhr1a$^{-/-}$ retinal cryosections probed with actin-antibodies (white) at various timepoints detecting cone CPs. Typical length of CPs observed is demonstrated in magenta. **F-J)** Confocal microscopy of wildtype retinal cryosections probed with actin-antibodies (white) and gnb1 (A') (magenta) at various timepoints detecting rod CPs. Typical length of CPs observed is demonstrated in yellow. **F'-J')** Confocal microscopy of cdhr1a$^{-/-}$ retinal cryosections probed with actin-antibodies (white) and gnb1 (F') (magenta) at various timepoints detecting rod CPs. Typical length of CPs observed is demonstrated in yellow. ROS = cone outer segment layer. **K)** Quantification of cone cells CP length based on measurements of actin staining in wildtype (black) compared to cdhr1a$^{-/-}$ (blue) at 5, 15, 30, 90 and 180 dpf. Standard deviation is shown in red. ** = $p<0.01$, **** = $p<0.0001$. **L)** Quantification of rod cells CP length based on measurements of actin staining in wildtype (black) compared to

758 cdhr1a$^{-/-}$ (blue) at 5, 15, 30, 90 and 180 dpf. Standard deviation is shown in red. ns = not
759 significant, *** = p<0.001, **** = p<0.0001. **M)** Line graph depicting the long-term trend of cone
760 cells CP length changes between wildtype (black) and cdhr1a$^{-/-}$ (blue) over time. ** = p<0.01,
761 **** = p<0.0001. **N)** Line graph depicting the long-term trend of rod cells CP length changes
762 between wildtype (black) and cdhr1a$^{-/-}$ (blue) over time. ns = not significant, *** = p<0.001, **** =
763 p<0.0001. **O)** Confocal microscopy of wildtype (top panels) and cdhr1a$^{-/-}$ (bottom panels) retinal
764 cryosections probed with pcdh15b antibody (red) at various time points. Scale bar = 10μm. COS
765 = cone outer segment layer, ROS = rod outer segment layer.
766
767 **Figure 6:** <u>Loss of pcdh15b function leads to early cone OS defects and mis-localization of</u>
768 <u>cdhr1a.</u>
769
770 **A)** Diagrammatic representation of the CRISPR/Cas9 strategy for generating a pcdh15b loss of
771 function allele. crRNAs were targeted to the flanking sequences of exon 5 and resulted in a
772 heritable deletion of 68bp which resulted in a frameshift (fs) at AA117 and a premature stop
773 codon (*) at AA118. **B-B")** Confocal microscopy of retinal cryosections from wildtype, pcdh15b$^{+/-}$
774 and pcdh15b$^{-/-}$individuals probed with pcdh15b antibody (red). Scale bar = 10μm.**C-D")**
775 Confocal microscopy of retinal cryosections from wildtype, pcdh15b$^{+/-}$ and pcdh15b$^{-/-}$ individuals
776 probed with prhp2 antibody (green) to visualize the cone outer segments (COS) at 5dpf (C-C")
777 and 10dpf (D-D"). Scale bar = 10μm.**E)** Quantification of COS length using prph2 signal for each
778 genotype at each time point is depicted on the right. Standard deviation is shown in red. ns =
779 not significant, ** = p<0.01. **** = p>0.0001. ANOVA = p<0.0001. **F-G")** Confocal microscopy of
780 retinal cryosections from wildtype, pcdh15b$^{+/-}$ and pcdh15b$^{-/-}$ individuals probed with actin
781 antibody (white) to visualize cone CPs at 5dpf (F-F") and 10dpf (G-G"). Scale bar = 10μm.**H)**
782 Quantification of CP length using actin signal for each genotype at each time point is depicted
783 on the right. Standard deviation is shown in red. ns = not significant, ** = p<0.01. **** =
784 p>0.0001. ANOVA = p<0.0001. **I-J")** Confocal microscopy of retinal cryosections from wildtype,
785 pcdh15b$^{+/-}$ and pcdh15b$^{-/-}$ individuals probed with cdhr1a antibody (red) at 5dpf (I-I") and 10dpf
786 (J-J"). White boxes indicate regions enlarged. Scale bar = 10μm.**K)** Quantification of cdhr1a OS
787 length for each genotype at each time point is depicted on the right. Standard deviation is shown
788 in red. ns = not significant, *** = p<0.001. **** = p>0.0001. ANOVA = p<0.0001.
789
790
791 **Figure 7:** <u>Cone phenotypes are exacerbated by simultaneous loss of pcdh15b and cdhr1a.</u>
792
793 **A-D)** Confocal microscopy of retinal cryosections from 5 dpf pcdh15b$^{-/-}$, cdhr1a$^{-/-}$, cdhr1a$^{-/-}$;
794 pcdh15b$^{+/-}$ and cdhr1a$^{-/-}$; pcdh15b$^{-/-}$ larva probed with prph2 antibodies (green). COS = cone
795 outer segment. Scale bar = 10μm. **E-H)** Confocal microscopy of retinal cryosections from 10 dpf
796 pcdh15b$^{-/-}$, cdhr1a$^{-/-}$, cdhr1a$^{-/-}$; pcdh15b$^{+/-}$ and cdhr1a$^{-/-}$; pcdh15b $^{-/-}$ larva probed with prph2
797 antibodies (green). COS = cone outer segment. Scale bar = 10μm. **I)** Quantification of cone
798 outer segment length at 5 dpf based on prph2 signal. ns = not significant, **** =p<0.0001.
799 ANOVA = p<0.0001. **J)** Quantification of cone outer segment length at 10 dpf based on prph2
800 signal. ns = not significant, ** = p< 0.01****, =p<0.0001. ANOVA = p<0.0001. **K-N)** Confocal
801 microscopy of retinal cryosections from 5 dpf pcdh15b$^{-/-}$, cdhr1a$^{-/-}$, cdhr1a$^{-/-}$; pcdh15b$^{+/-}$ and
802 cdhr1a$^{-/-}$; pcdh15b $^{-/-}$ larva probed with actin antibodies (white). COS = cone outer segment.
803 Scale bar = 10μm. **O-R)** Confocal microscopy of retinal cryosections from 10 dpf pcdh15b$^{-/-}$,
804 cdhr1a$^{-/-}$, cdhr1a$^{-/-}$; pcdh15b$^{+/-}$ and cdhr1a$^{-/-}$; pcdh15b$^{-/-}$larva probed with actin antibodies
805 (white). COS = cone outer segment. Scale bar = 10μm. **R)** Quantification of cone CP length at 5
806 dpf based on prph2 signal. ns = not significant, **** =p<0.0001. ANOVA = p<0.0001. **T)**

807 Quantification of cone CP length at 10 dpf based on prph2 signal. ns = not significant, * = p<
808 0.05 ** = p< 0.01****, =p<0.0001. ANOVA = p<0.0001.
809
810
811 **Supplementary figure 1:** Expression of USHR genes in the zebrafish retina.
812 Whole mount in situ hybridization of 5 dpf zebrafish larva for **A)** *cdhr1a*, **B)** *pcdh15b*, **C)** *pcdh23*,
813 **D)** *ush1ga*, **E)** *harmonin*, **F)** *myo7aa*. Ventral images of the embryos are displayed. White
814 arrows indicate expression in the outer nuclear layer of the retina.
815

816 **Supplementary Table 1:** WISH probe primer sets
817

Cdhr1a	ATGAAGAATGCAAGGGAAATA	TAATACGACTCACTATAGGGTCCTTCTGGACTGATTTCCAATGC
Pcdh15b	GGTGATGGATCCAGTTCAGTG	TAATACGACTCACTATAGGGTCACAGAACAGTGGACTGAGA
pcdh23	AGTGATTCAGATGATCGACGA	TAATACGACTCACTATAGGGTCATAACTCTGTGATCTCTAA
Harmonin	CCTTAGTTTGGTGGGCACCAA	TAATACGACTCACTATAGGGTTAAAAGAATGTCACCTCATC
Ush1ga	TTCTTGCCTTAATGTCTGTTT	TAATACGACTCACTATAGGGGCGCAGCTTTCACAAAACCAT
Myo7aa	AAACAAGGACATTTTAACCAC	TAATACGACTCACTATAGGGGAGTCACATCGATCACTGGAC

818
819

REFERENCES

1 Ackland, P., Resnikoff, S. & Bourne, R. World blindness and visual impairment: despite many successes, the problem is growing. *Community Eye Health* **30**, 71-73 (2017).

2 L, S., Bowne, S. & Diager, S. *RetNet - Retinal Information Network*, <https://web.sph.uth.edu/RetNet/> (2020).

3 Arno, G. *et al.* Reevaluation of the Retinal Dystrophy Due to Recessive Alleles of RGR With the Discovery of a Cis-Acting Mutation in CDHR1. *Invest Ophthalmol Vis Sci* **57**, 4806-4813, doi:10.1167/iovs.16-19687 (2016).

4 Duncan, J. L. *et al.* Identification of a novel mutation in the CDHR1 gene in a family with recessive retinal degeneration. *Arch Ophthalmol* **130**, 1301-1308, doi:10.1001/archophthalmol.2012.1906 (2012).

5 Stingl, K. *et al.* CDHR1 mutations in retinal dystrophies. *Sci Rep* **7**, 6992, doi:10.1038/s41598-017-07117-8 (2017).

6 Rattner, A. *et al.* A photoreceptor-specific cadherin is essential for the structural integrity of the outer segment and for photoreceptor survival. *Neuron* **32**, 775-786, doi:10.1016/s0896-6273(01)00531-1 (2001).

7 Yusuf, I. H., McClements, M. E., MacLaren, R. E. & Charbel Issa, P. Deep phenotyping of the Cdhr1. *Exp Eye Res* **208**, 108603, doi:10.1016/j.exer.2021.108603 (2021).

8 Burgoyne, T. *et al.* Rod disc renewal occurs by evagination of the ciliary plasma membrane that makes cadherin-based contacts with the inner segment. *Proc Natl Acad Sci U S A* **112**, 15922-15927, doi:10.1073/pnas.1509285113 (2015).

9 Rattner, A., Chen, J. & Nathans, J. Proteolytic shedding of the extracellular domain of photoreceptor cadherin. Implications for outer segment assembly. *J Biol Chem* **279**, 42202-42210, doi:10.1074/jbc.M407928200 (2004).

10 Carr, B. J., Stanar, P. & Moritz, O. L. Distinct roles for prominin-1 and photoreceptor cadherin in outer segment disc morphogenesis in CRISPR-altered X. laevis. *J Cell Sci* **134**, doi:10.1242/jcs.253906 (2021).

11 Ba-Abbad, R. *et al.* A clinical study of patients with novel CDHR1 genotypes associated with late-onset macular dystrophy. *Eye (Lond)* **35**, 1482-1489, doi:10.1038/s41433-020-1045-3 (2021).

12 Bolz, H., Ebermann, I. & Gal, A. Protocadherin-21 (PCDH21), a candidate gene for human retinal dystrophies. *Mol Vis* **11**, 929-933 (2005).

13 Ostergaard, E., Batbayli, M., Duno, M., Vilhelmsen, K. & Rosenberg, T. Mutations in PCDH21 cause autosomal recessive cone-rod dystrophy. *J Med Genet* **47**, 665-669, doi:10.1136/jmg.2009.069120 (2010).

14 Aberle, H., Schwartz, H. & Kemler, R. Cadherin-catenin complex: protein interactions and their implications for cadherin function. *J Cell Biochem* **61**, 514-523, doi:10.1002/(sici)1097-4644(19960616)61:4%3c514::Aid-jcb4%3e3.0.Co;2-r (1996).

15 Yang, Z. *et al.* Mutant prominin 1 found in patients with macular degeneration disrupts photoreceptor disk morphogenesis in mice. *J Clin Invest* **118**, 2908-2916, doi:10.1172/jci35891 (2008).

16 Hirano, S., Nose, A., Hatta, K., Kawakami, A. & Takeichi, M. Calcium-dependent cell-cell adhesion molecules (cadherins): subclass specificities and possible involvement of actin bundles. *J Cell Biol* **105**, 2501-2510, doi:10.1083/jcb.105.6.2501 (1987).

17 Takeichi, M., Shirayoshi, Y., Hatta, K. & Nose, A. Cadherins: their morphogenetic role in animal development. *Prog Clin Biol Res* **217B**, 17-27 (1986).

18 Pancho, A., Aerts, T., Mitsogiannis, M. D. & Seuntjens, E. Protocadherins at the Crossroad of Signaling Pathways. *Front Mol Neurosci* **13**, 117, doi:10.3389/fnmol.2020.00117 (2020).

19 Halbleib, J. M. & Nelson, W. J. Cadherins in development: cell adhesion, sorting, and tissue morphogenesis. *Genes Dev* **20**, 3199-3214, doi:10.1101/gad.1486806 (2006).

20 COHEN, A. I. The fine structure of the extrafoveal receptors of the Rhesus monkey. *Exp Eye Res* **1**, 128-136, doi:10.1016/s0014-4835(61)80018-3 (1961).

21 Burnside, B. Thin (actin) and thick (myosinlike) filaments in cone contraction in the teleost retina. *J Cell Biol* **78**, 227-246, doi:10.1083/jcb.78.1.227 (1978).

22 Chaitin, M. H. & Bok, D. Immunoferritin localization of actin in retinal photoreceptors. *Invest Ophthalmol Vis Sci* **27**, 1764-1767 (1986).

23 Sahly, I. *et al.* Localization of Usher 1 proteins to the photoreceptor calyceal processes, which are absent from mice. *J Cell Biol* **199**, 381-399, doi:10.1083/jcb.201202012 (2012).

24 Sharkova, M., Aparicio, G., Mouzaaber, C., Zolessi, F. R. & Hocking, J. C. Photoreceptor calyceal processes accompany the developing outer segment, adopting a stable length despite a dynamic core. *J Cell Sci* **137**, doi:10.1242/jcs.261721 (2024).

25 COHEN, A. I. The ultrastructure of the rods of the mouse retina. *Am J Anat* **107**, 23-48, doi:10.1002/aja.1001070103 (1960).

26 Mathur, P. & Yang, J. Usher syndrome: Hearing loss, retinal degeneration and associated abnormalities. *Biochim Biophys Acta* **1852**, 406-420, doi:10.1016/j.bbadis.2014.11.020 (2015).

27 Kazmierczak, P. *et al.* Cadherin 23 and protocadherin 15 interact to form tip-link filaments in sensory hair cells. *Nature* **449**, 87-91, doi:10.1038/nature06091 (2007).

28 Goldberg, A. F. Role of peripherin/rds in vertebrate photoreceptor architecture and inherited retinal degenerations. *Int Rev Cytol* **253**, 131-175, doi:10.1016/s0074-7696(06)53004-9 (2006).

29 McPherson, D. R. Sensory Hair Cells: An Introduction to Structure and Physiology. *Integr Comp Biol* **58**, 282-300, doi:10.1093/icb/icy064 (2018).

30 Lelli, A., Kazmierczak, P., Kawashima, Y., Müller, U. & Holt, J. R. Development and regeneration of sensory transduction in auditory hair cells requires functional interaction between cadherin-23 and protocadherin-15. *J Neurosci* **30**, 11259-11269, doi:10.1523/jneurosci.1949-10.2010 (2010).

31 Miles, A., Blair, C., Emili, A. & Tropepe, V. Usher syndrome type 1-associated gene, pcdh15b, is required for photoreceptor structural integrity in zebrafish. *Dis Model Mech* **14**, doi:10.1242/dmm.048965 (2021).

32 Schietroma, C. *et al.* Usher syndrome type 1-associated cadherins shape the photoreceptor outer segment. *J Cell Biol* **216**, 1849-1864, doi:10.1083/jcb.201612030 (2017).

33 Schreiner, D. & Weiner, J. A. Combinatorial homophilic interaction between gamma-protocadherin multimers greatly expands the molecular diversity of cell adhesion. *Proc Natl Acad Sci U S A* **107**, 14893-14898, doi:10.1073/pnas.1004526107 (2010).

34 Yusuf, I. H., McClements, M. E., MacLaren, R. E. & Charbel Issa, P. Deep phenotyping of the Cdhr1(-/-) mouse validates its use in pre-clinical studies for human CDHR1-associated retinal degeneration. *Exp Eye Res* **208**, 108603, doi:10.1016/j.exer.2021.108603 (2021).

35 Piedade, W. P., Titialii-Torres, K., Morris, A. C. & Famulski, J. K. Proteasome-Mediated Regulation of Cdhr1a by Siah1 Modulates Photoreceptor Development and Survival in Zebrafish. *Front Cell Dev Biol* **8**, 594290, doi:10.3389/fcell.2020.594290 (2020).

36 Elferich, J. *et al.* Molecular structures and conformations of protocadherin-15 and its complexes on stereocilia elucidated by cryo-electron tomography. *Elife* **10**, doi:10.7554/eLife.74512 (2021).

37 Piedade, W. P. & Famulski, J. K. E3 ubiquitin ligase-mediated regulation of vertebrate ocular development; new insights into the function of SIAH enzymes. *Biochem Soc Trans* **49**, 327-340, doi:10.1042/BST20200613 (2021).

38 Holly, V. L., Widen, S. A., Famulski, J. K. & Waskiewicz, A. J. Sfrp1a and Sfrp5 function as positive regulators of Wnt and BMP signaling during early retinal development. *Dev Biol* **388**, 192-204, doi:10.1016/j.ydbio.2014.01.012 (2014).

39 Pereira Piedade, W., Veith, S. & Famulski, J. K. Ubiquitin-mediated proteasome degradation regulates optic fissure fusion. *Biol Open* **8**, doi:10.1242/bio.044974 (2019).

40 Hoshijima, K. *et al.* Highly Efficient CRISPR-Cas9-Based Methods for Generating Deletion Mutations and F0 Embryos that Lack Gene Function in Zebrafish. *Dev Cell* **51**, 645-657.e644, doi:10.1016/j.devcel.2019.10.004 (2019).

Figure 1

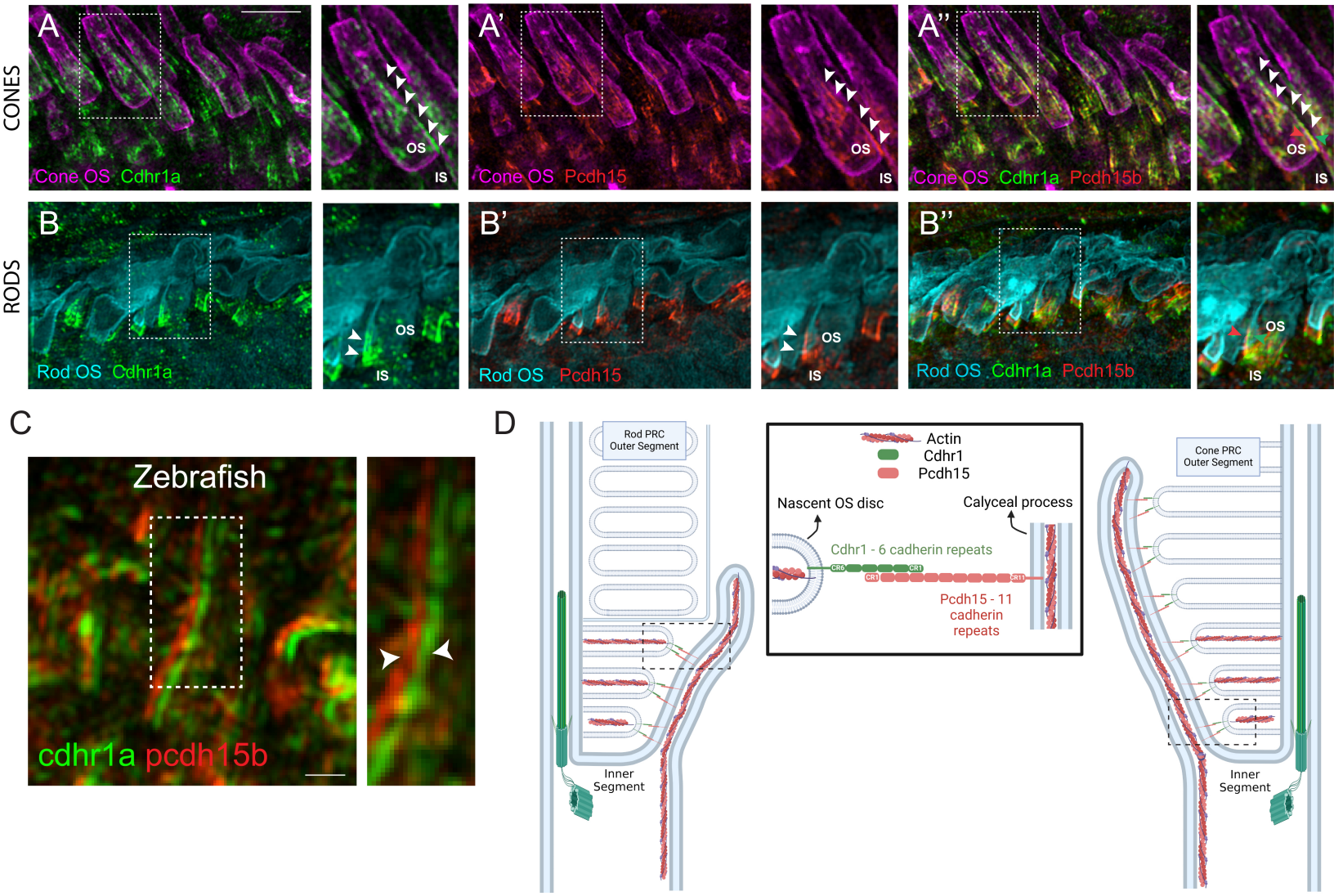
CONES
RODS
A
A'
A''
B
B'
B''
Cone OS Cdhr1a
Cone OS Pcdh15
Cone OS Cdhr1a Pcdh15b
Rod OS Cdhr1a
Rod OS Pcdh15
Rod OS Cdhr1a Pcdh15b
OS
IS
C
Zebrafish
cdhr1a pcdh15b
D
Rod PRC Outer Segment
Cone PRC Outer Segment
Inner Segment
Actin
Cdhr1
Pcdh15
Nascent OS disc
Calyceal process
Cdhr1 - 6 cadherin repeats
Pcdh15 - 11 cadherin repeats

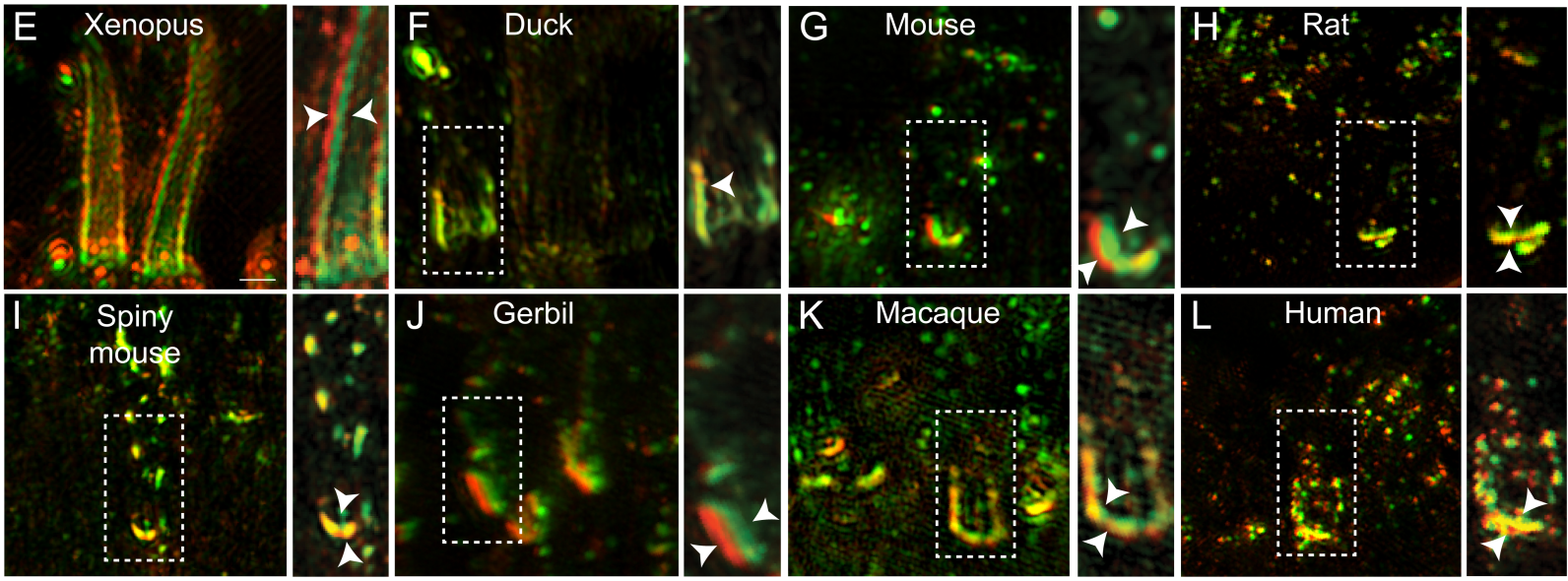
E Xenopus
F Duck
G Mouse
H Rat
I Spiny mouse
J Gerbil
K Macaque
L Human

Figure 2

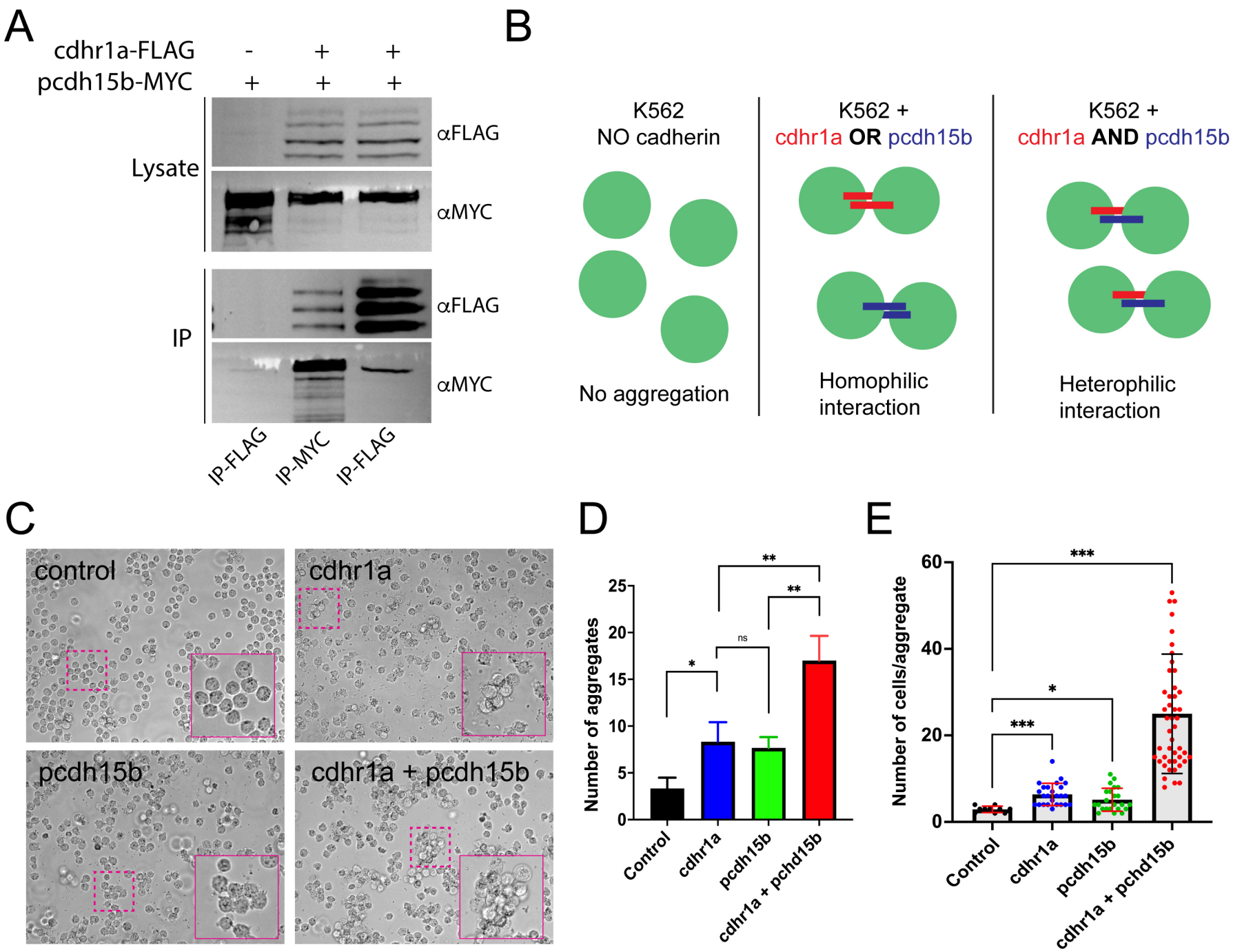
A
cdhr1a-FLAG - + +
pcdh15b-MYC + + +
Lysate
αFLAG
αMYC
IP
αFLAG
αMYC
IP-FLAG
IP-MYC
IP-FLAG
B
K562
NO cadherin
No aggregation
K562 +
cdhr1a OR pcdh15b
Homophilic interaction
K562 +
cdhr1a AND pcdh15b
Heterophilic interaction
C
control
cdhr1a
pcdh15b
cdhr1a + pcdh15b
D
Number of aggregates
25
20
15
10
5
0
*
ns
**
**
Control
cdhr1a
pcdh15b
cdhr1a + pchd15b
E
Number of cells/aggregate
60
40
20
0
***
*
***
Control
cdhr1a
pcdh15b
cdhr1a + pchd15b

Figure 3

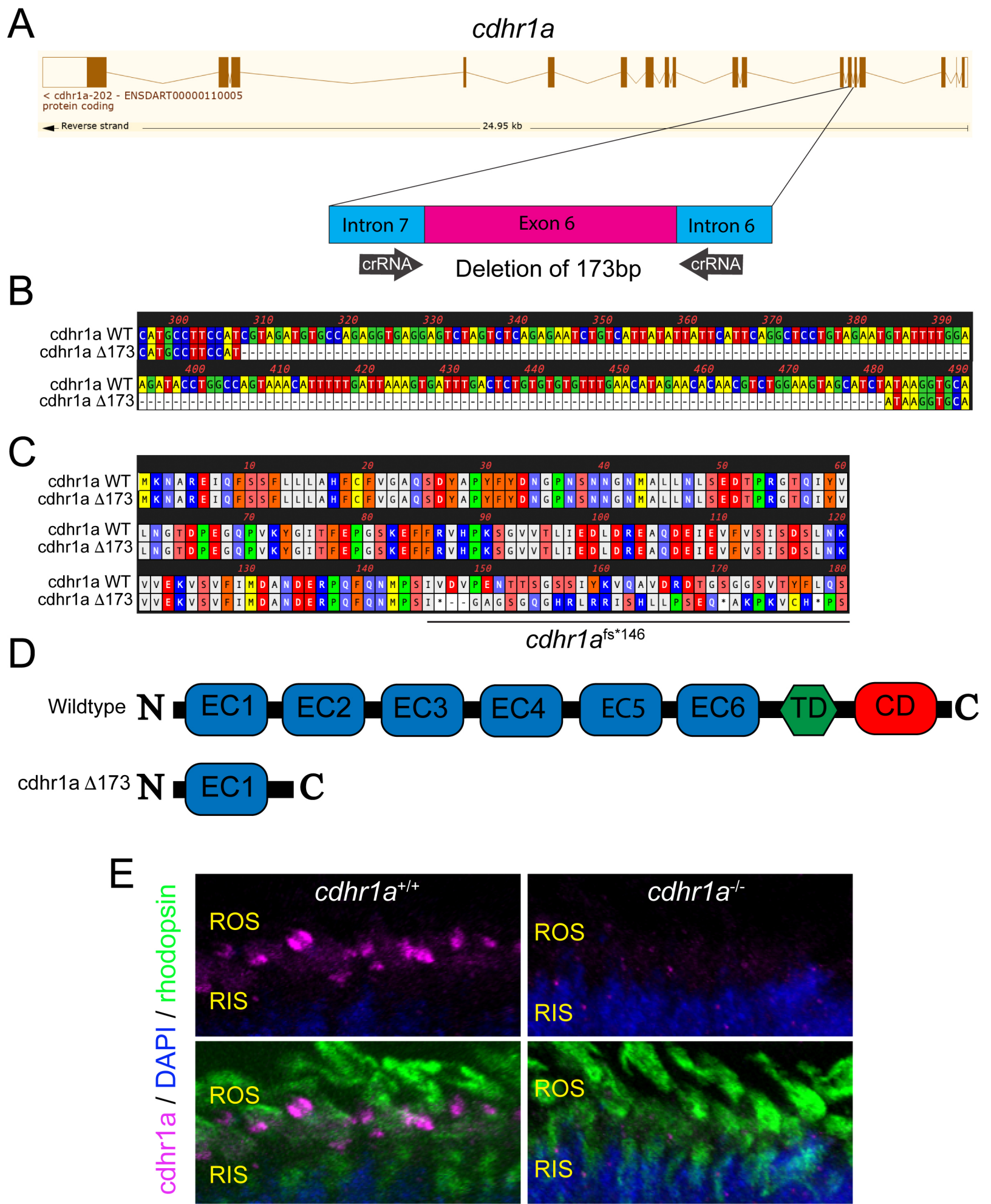
A
cdhr1a
< cdhr1a-202 - ENSDART00000110005
protein coding
Reverse strand
24.95 kb
Intron 7
Exon 6
Intron 6
crRNA
Deletion of 173bp
crRNA
B
cdhr1a WT
cdhr1a Δ173
C
cdhr1a WT
cdhr1a Δ173
cdhr1a fs*146
D
Wildtype
N
EC1
EC2
EC3
EC4
EC5
EC6
TD
CD
C
cdhr1a Δ173
N
EC1
C
E
cdhr1a+/+
cdhr1a-/-
ROS
RIS
cdhr1a / DAPI / rhodopsin

Figure 4

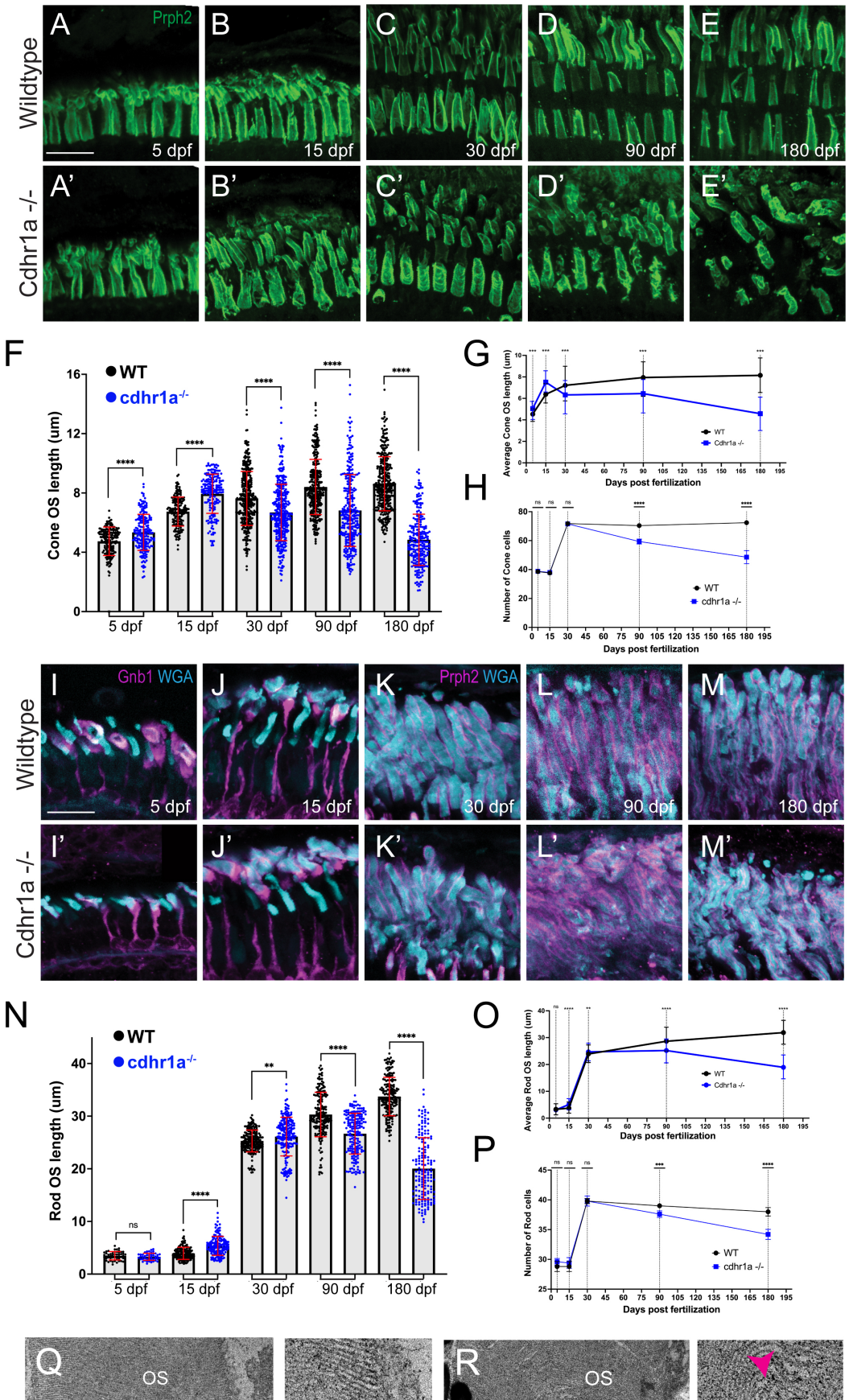
A
Prph2
B
C
D
E
Wildtype
5 dpf
15 dpf
30 dpf
90 dpf
180 dpf
A'
B'
C'
D'
E'
Cdhr1a -/-
F
WT
cdhr1a-/-
Cone OS length (um)
5 dpf
15 dpf
30 dpf
90 dpf
180 dpf
G
Average Cone OS length (um)
Days post fertilization
H
Number of Cone cells
Days post fertilization
I
Gnb1 WGA
J
K
Prph2 WGA
L
M
I'
J'
K'
L'
M'
N
Rod OS length (um)
O
Average Rod OS length (um)
P
Number of Rod cells
Q
OS
IS
WT 15dpf
R
cdhr1a-/- 15dpf

Figure 5

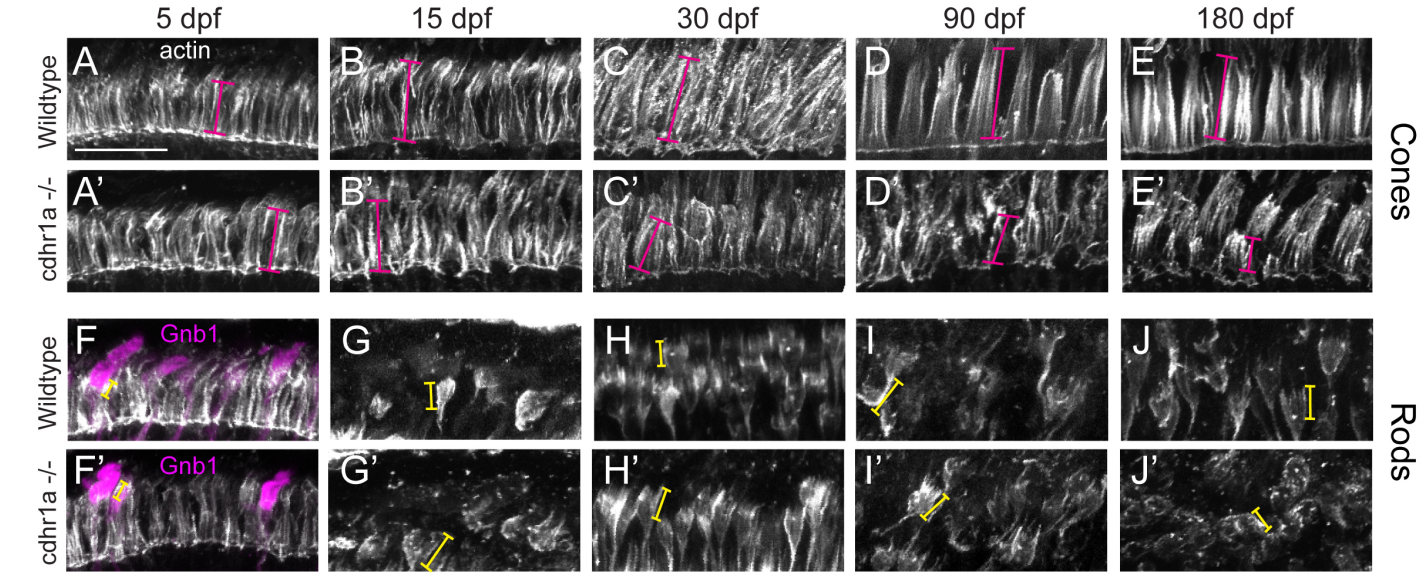
5 dpf
15 dpf
30 dpf
90 dpf
180 dpf
Wildtype
cdhr1a -/-
actin
Gnb1
Cones
Rods

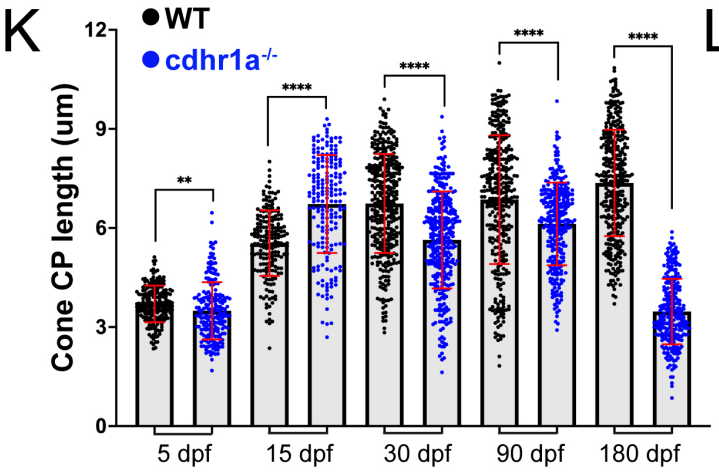
K
WT
cdhr1a-/-
Cone CP length (um)
5 dpf
15 dpf
30 dpf
90 dpf
180 dpf

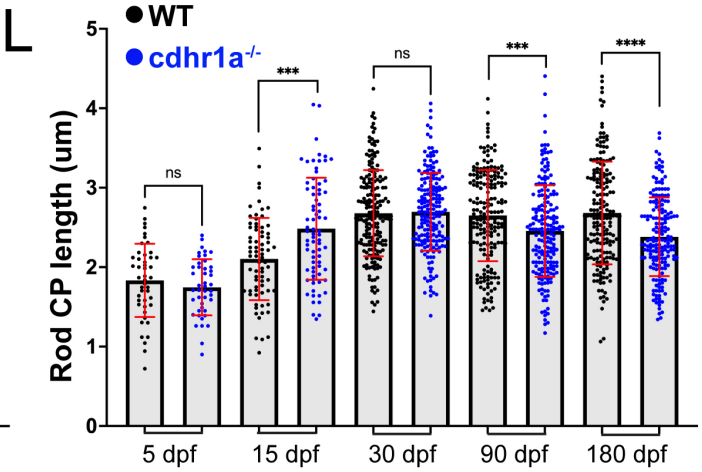
L
WT
cdhr1a-/-
Rod CP length (um)
5 dpf
15 dpf
30 dpf
90 dpf
180 dpf

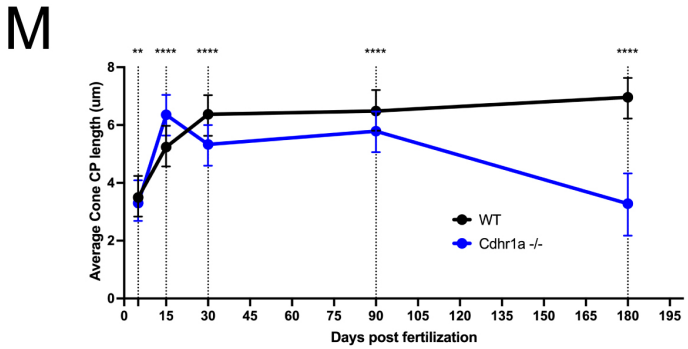
M
Average Cone CP length (um)
WT
Cdhr1a -/-
Days post fertilization

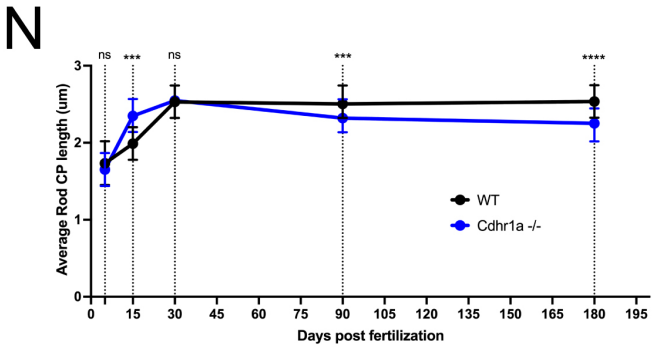
N
Average Rod CP length (um)
WT
Cdhr1a -/-
Days post fertilization

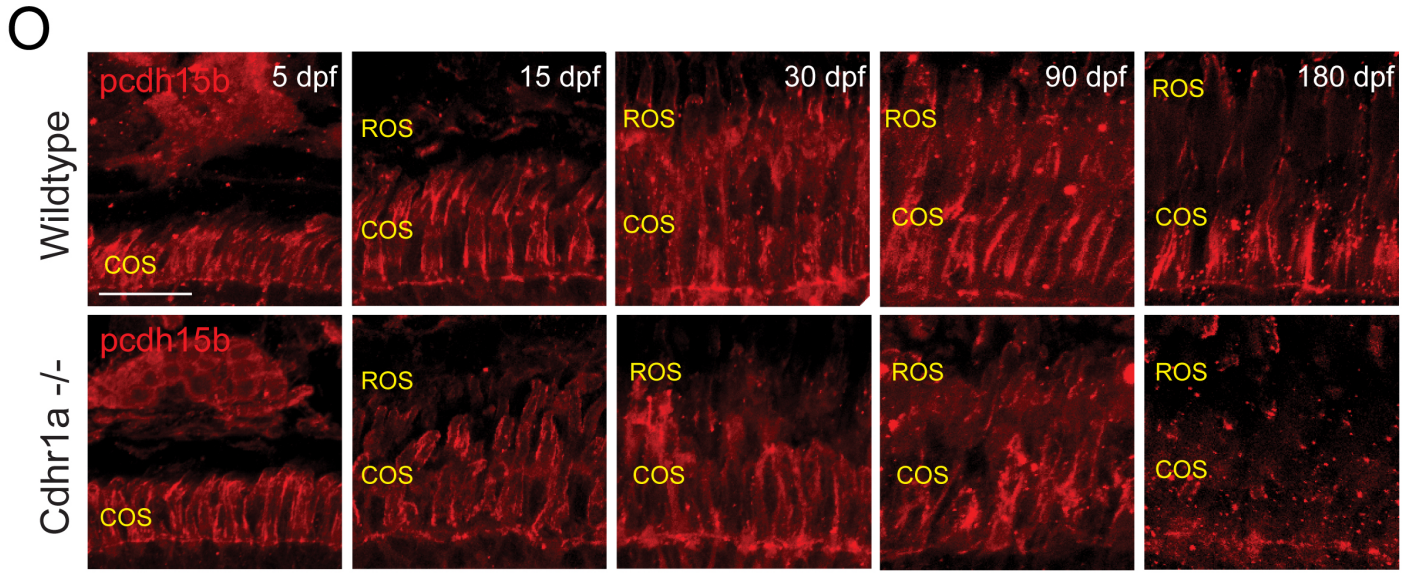
O
Wildtype
Cdhr1a -/-
pcdh15b
5 dpf
15 dpf
30 dpf
90 dpf
180 dpf
ROS
COS

Figure 6

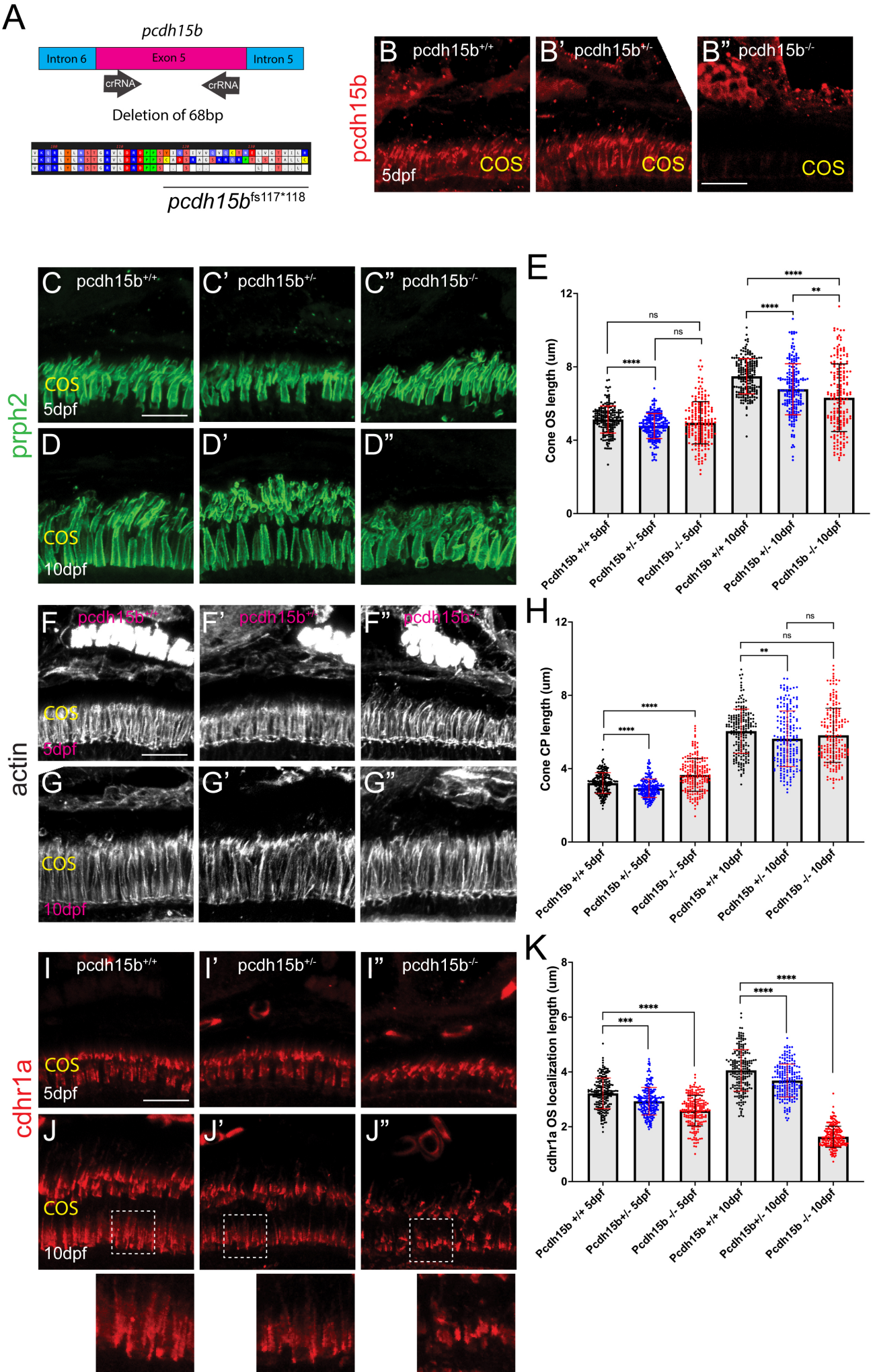
A
pcdh15b
Intron 6
Exon 5
Intron 5
crRNA
crRNA
Deletion of 68bp
pcdh15b fs117*118
B pcdh15b+/+
B' pcdh15b+/-
B" pcdh15b-/-
pcdh15b
5dpf
COS
C pcdh15b+/+
C' pcdh15b+/-
C" pcdh15b-/-
prph2
D
D'
D"
10dpf
E
Cone OS length (um)
Pcdh15b +/+ 5dpf
Pcdh15b +/- 5dpf
Pcdh15b -/- 5dpf
Pcdh15b +/+ 10dpf
Pcdh15b +/- 10dpf
Pcdh15b -/- 10dpf
F
F'
F"
actin
G
G'
G"
H
Cone CP length (um)
I pcdh15b+/+
I' pcdh15b+/-
I" pcdh15b-/-
cdhr1a
J
J'
J"
K
cdhr1a OS localization length (um)

Figure 7

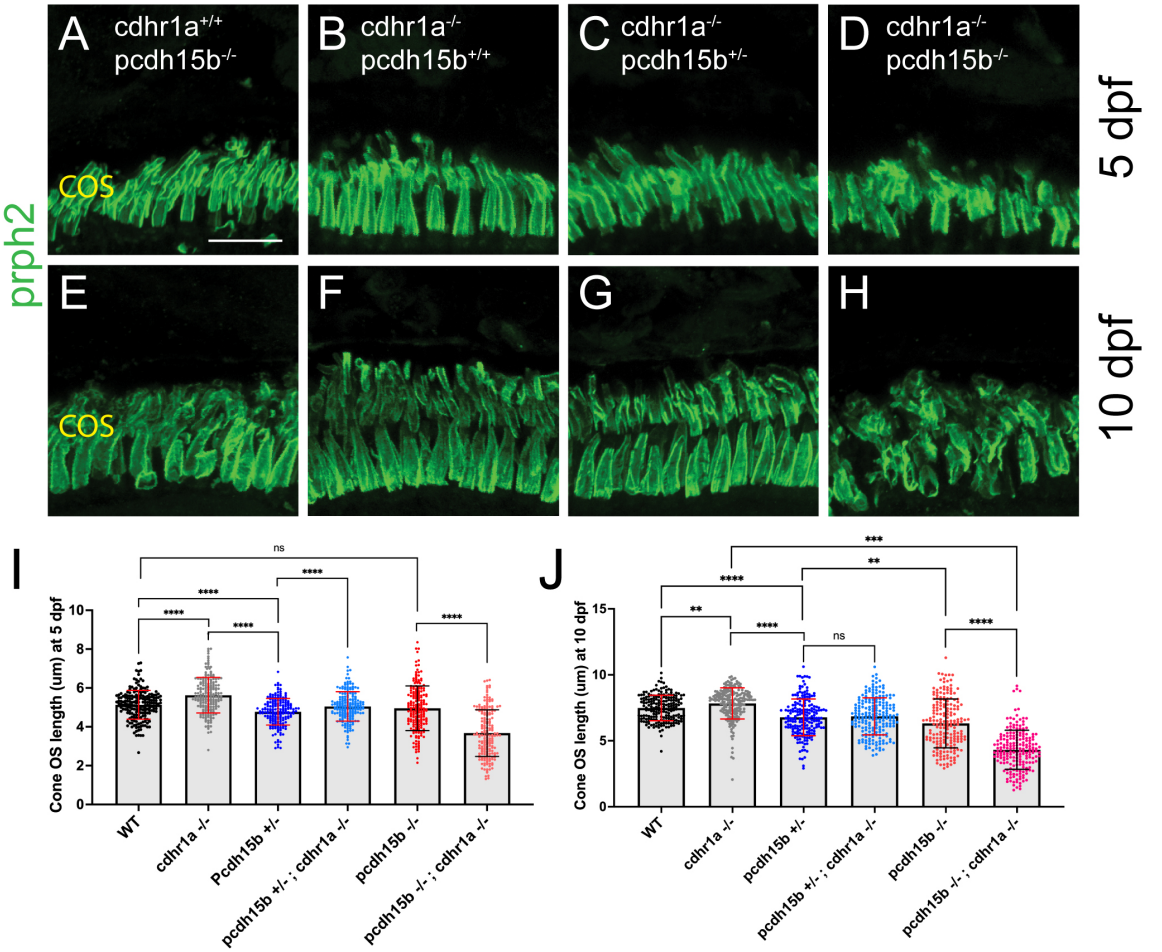
A cdhr1a+/+ pcdh15b-/-
B cdhr1a-/- pcdh15b+/+
C cdhr1a-/- pcdh15b+/-
D cdhr1a-/- pcdh15b-/-
5 dpf
prph2
COS
E
F
G
H
10 dpf
I
Cone OS length (um) at 5 dpf
WT
cdhr1a -/-
Pcdh15b +/-
pcdh15b +/- ; cdhr1a -/-
pcdh15b -/-
pcdh15b -/- ; cdhr1a -/-
J
Cone OS length (um) at 10 dpf

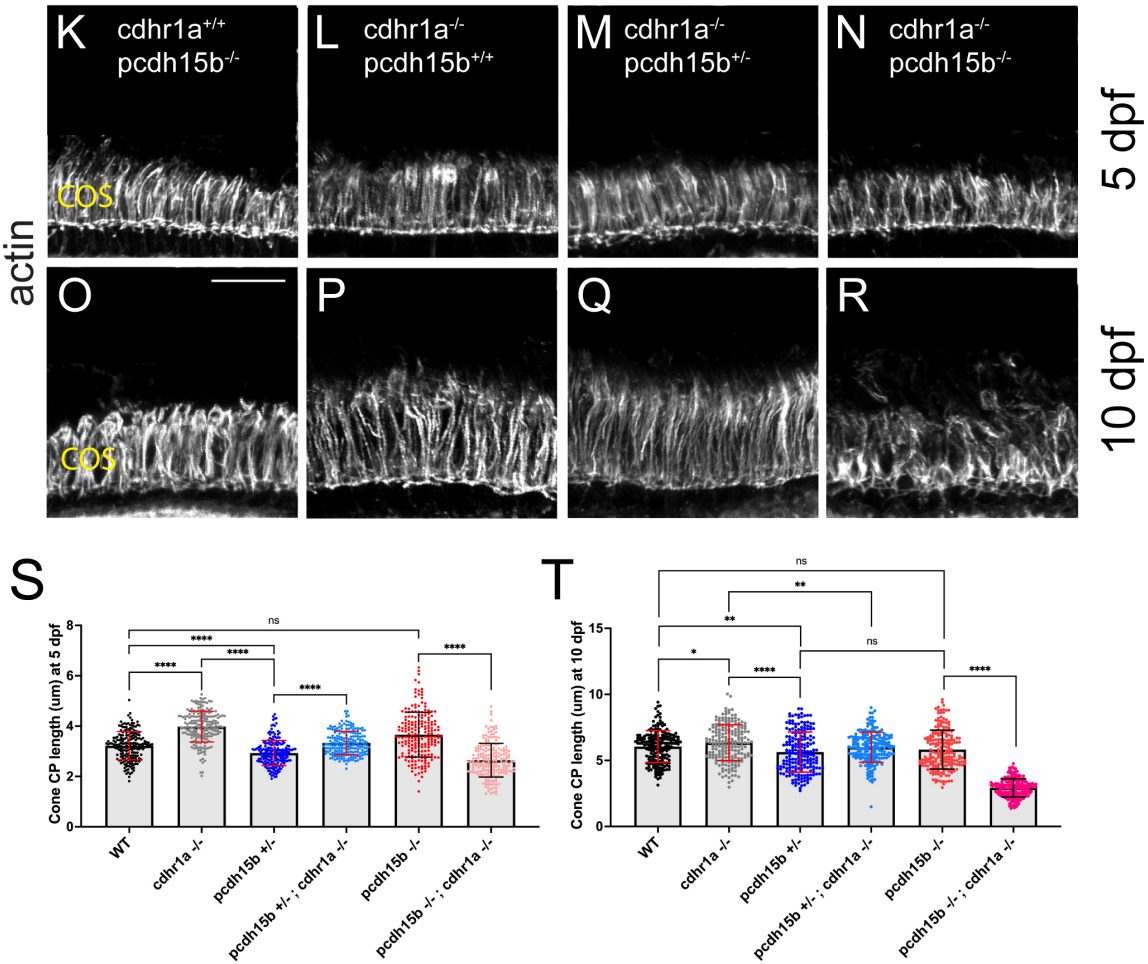
K cdhr1a+/+ pcdh15b-/-
L cdhr1a-/- pcdh15b+/+
M cdhr1a-/- pcdh15b+/-
N cdhr1a-/- pcdh15b-/-
5 dpf
actin
COS
O
P
Q
R
10 dpf
S
Cone CP length (um) at 5 dpf
WT
cdhr1a -/-
pcdh15b +/-
pcdh15b +/- ; cdhr1a -/-
pcdh15b -/-
pcdh15b -/- ; cdhr1a -/-
T
Cone CP length (um) at 10 dpf
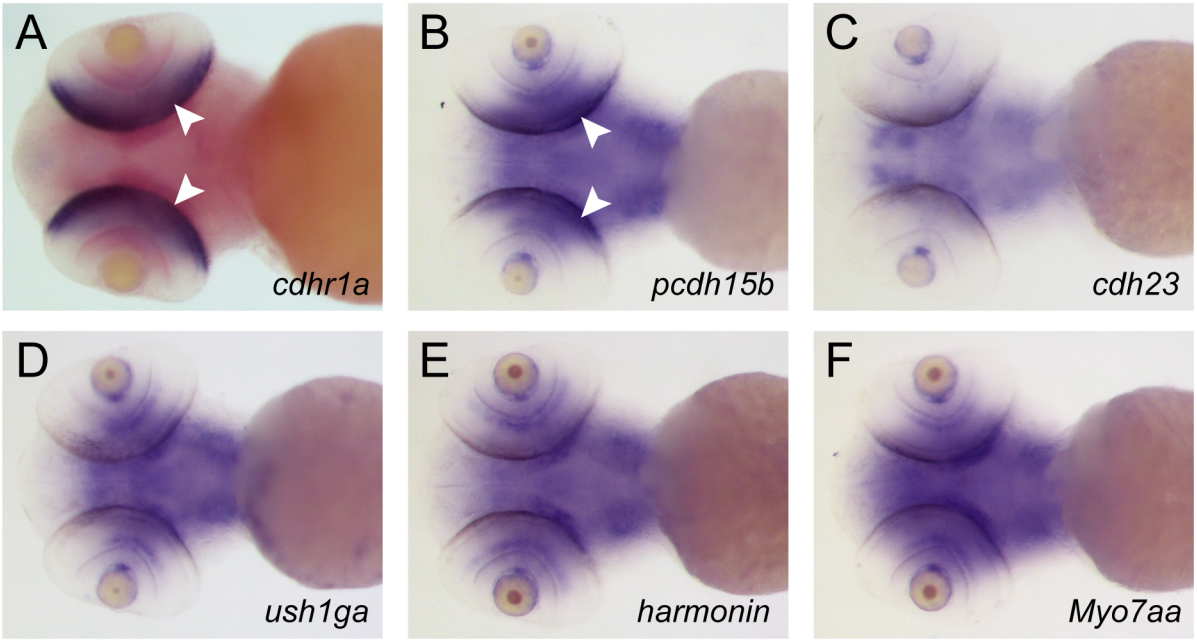
Supplemental Figure 1